Electronic Supporting Information: Quantum dynamics of the $\pi\pi^*$/nπ^* decay of the epigenetic nucleobase 1,5dimethyl-cytosine in gas phase.

Martha Yaghoubi Jouybari,† Yanli Liu,‡ Roberto Improta,*,¶ and Fabrizio Santoro*,†

†*CNR–Consiglio Nazionale delle Ricerche, Istituto di Chimica dei Composti Organo Metallici (ICCOM-CNR), SS di Pisa, Area della Ricerca, via G. Moruzzi 1, I-56124 Pisa, Italy*

‡*School of Physics and Optoelectronics Engineering, Ludong University, 264025 Yantai, Shandong, PR China*

¶*CNR-Consiglio Nazionale delle Ricerche, Istituto di Biostrutture e Bioimmagini (IBB-CNR), via Mezzocannone 16, I-80136 Napoli, Italy*

E-mail: robimp@unina.it; fabrizio.santoro@pi.iccom.cnr.it

Contents

S1 Additional static results

S1.1 CAM-B3LYP

S1.1.1 Optimized geometries (C_S symmetry) of the ground and excited states and their normal modes with imaginary frequencies, bond distances and angles

The structures we report in the following of $\pi_H\pi_L^*$ and $n_N\pi_L^*$ correspond to minima on the lowest adiabatic PES (S1) (the former more stable than the latter). At variance, the structure $n_O\pi_L^*$ corresponds to a minimum on the second adiabatic PES (S2) and, finally, $\pi_1\pi_L^*$ is a minimum on the third adiabatic state (S3). Excited state energies at the different stationary points are reported in sections S1.1.2-S1.1.5.

Table S1: Cartesian coordinates of 1,5diMe-Cyt at the ground state (GS) minimum. CAM-B3LYP/6-31+G(d,p) calculations in gas phase.

1,5diMe-Cyt-Minimum of GS			
C	0.000000	1.301380	0.000000
C	-1.244384	-0.769301	0.000000
C	1.084188	-0.787028	0.000000
C	1.189778	0.650364	0.000000
N	-1.187514	0.647663	0.000000
N	-0.054957	-1.438918	0.000000
N	2.217677	-1.533302	0.000000
O	-2.343659	-1.303882	0.000000
H	-0.054322	2.385616	0.000000
H	3.134977	-1.123679	0.000000
H	2.118000	-2.536571	0.000000
C	2.510867	1.363127	0.000000
H	3.108772	1.117607	0.885640
H	3.108772	1.117607	-0.885640
H	2.364560	2.446012	0.000000
C	-2.459023	1.357823	0.000000
H	-3.040360	1.083408	-0.881940
H	-3.040360	1.083408	0.881940
H	-2.265769	2.431344	0.000000

Table S2: Cartesian coordinates of 1,5diMe-Cyt at the minimum of the first $\pi\pi^*$ state (character $\pi_H\pi_L^*$). CAM-B3LYP/6-31+G(d,p) calculations in gas phase.

1,5diMe-Cyt-Minimum of $\pi_H\pi_L^*$			
C	-1.211932	0.600985	0.000000
C	0.117400	-1.405807	0.000000
C	1.201615	0.645018	0.000000
C	0.000000	1.345140	0.000000
N	-1.142111	-0.771938	0.000000
N	1.257095	-0.732885	0.000000
N	2.428753	1.254574	0.000000
O	0.067850	-2.661060	0.000000
H	-2.188600	1.061110	0.000000
H	2.539854	2.251884	0.000000
H	3.243712	0.664474	0.000000
C	-0.047795	2.837305	0.000000
H	0.454344	3.251807	0.883672
H	0.454344	3.251807	-0.883672
H	-1.076406	3.203644	0.000000
C	-2.354884	-1.575590	0.000000
H	-2.396086	-2.212973	-0.885307
H	-2.396086	-2.212973	0.885307
H	-3.210461	-0.900857	0.000000

Table S3: Cartesian coordinates of 1,5diMe-Cyt at the minimum of the first nπ^* state (character $n_N\pi_L^*$). CAM-B3LYP/6-31+G(d,p) calculations in gas phase.

1,5diMe-Cyt-Minimum of First nπ^*			
C	-0.068149	1.308873	0.000000
C	-1.264464	-0.833629	0.000000
C	1.233708	-0.691054	0.000000
C	1.174110	0.705305	0.000000
N	-1.267375	0.569964	0.000000
N	0.000000	-1.288895	0.000000
N	2.350876	-1.487807	0.000000
O	-2.288938	-1.495762	0.000000
H	-0.183890	2.382672	0.000000
H	3.266070	-1.076206	0.000000
H	2.267714	-2.488252	0.000000
C	2.449501	1.505952	0.000000
H	3.058882	1.299838	0.887053
H	3.058882	1.299838	-0.887053
H	2.221520	2.573795	0.000000
C	-2.568464	1.214403	0.000000
H	-3.144476	0.934586	-0.885696
H	-3.144476	0.934586	0.885696
H	-2.410693	2.293297	0.000000

Table S4: Cartesian coordinates of 1,5diMe-Cyt at the minimum of the second nπ^* state (character $n_O\pi^*_L$). CAM-B3LYP/6-31+G(d,p) calculations in gas phase.

1,5diMe-Cyt-Minimum of Second nπ^*			
C	1.164709	0.701390	0.000000
C	0.000000	-1.343098	0.000000
C	-1.221492	0.585627	0.000000
C	-0.075281	1.346101	0.000000
N	1.190056	-0.715679	0.000000
N	-1.159938	-0.815570	0.000000
N	-2.501315	1.078242	0.000000
O	0.047770	-2.665363	0.000000
H	2.120162	1.200052	0.000000
H	-2.693186	2.063196	0.000000
H	-3.264855	0.424815	0.000000
C	2.432679	-1.467728	0.000000
H	2.512915	-2.097316	0.890683
H	2.512915	-2.097316	-0.890683
H	3.261072	-0.761104	0.000000
C	-0.143594	2.848365	0.000000
H	-0.666615	3.227159	-0.885818
H	-0.666615	3.227159	0.885818
H	0.858295	3.283368	0.000000

Table S5: Normal modes and imaginary frequencies of 1,5diMe-Cyt calculated at different stationary points (FC is the ground state minimum, for other geometries the character of the state with vanishing gradient is given), computed at CAM-B3LYP/6-31+G(d,p) level.

Geometries	mode	ω (cm^{-1})	description
FC	1	i93.21	NH_2 pyramidalization bending out-of plane
$\pi_H\pi^*_L$	1	i401.24	NH_2 pyramidalization bending out-of plane
	2	i210.60	Methyl rotation
	3	i63.12	ring out of plane
n$_N\pi^*_L$	1	i510.88	NH_2 pyramidalization bending out-of plane
	2	i167.02	ring out of plane and Methyl rotation
	3	i157.00	ring out of plane and Methyl rotation
	4	i20.34	ring out of plane and Methyl rotation
n$_O\pi^*_L$	1	i422.318	NH_2 pyramidalization bending out-of plane
	2	i178.10	Methyl rotation and ring out of plane

Table S6: Selected bond distances and angles of 1,5diMe-Cyt in optimized minima (constrained to C$_s$ symmetry) of the adiabatic surfaces calculated at CAM-B3LYP/6-31+G(d,p) in the gas phase. The structures are labelled with the diabatic character of the optimized states in the located minimum.

Bond	$\pi_H\pi^*_L$	n$_N\pi^*_L$	$\pi_1\pi^*_L$	n$_O\pi^*_L$	Angles	$\pi_H\pi^*_L$	n$_N\pi^*_L$	$\pi_1\pi^*_L$	n$_O\pi^*_L$
C6-N1	1.37	1.41	1.40	1.42	C6-N1-C2	119.63	121.52	124.60	116.77
N1-C2	1.41	1.40	1.41	1.35	N1-C2-N3	122.73	109.92	117.47	127.75
C2-N3	1.32	1.34	1.37	1.27	C2-N3-C4	118.25	134.34	117.12	116.97
N3-C4	1.38	1.37	1.39	1.40	N3-C4-C5	122.53	113.41	128.01	121.05
C4-C5	1.39	1.40	1.38	1.38	C4-C5-C6	118.22	118.36	114.60	118.97
C5-C6	1.42	1.38	1.41	1.40	C5-C6-N1	118.64	122.45	118.21	118.50
N1-C10	1.45	1.45	1.45	1.45	N8-C4-C5	123.36	127.94	124.26	125.38
C2-O7	1.26	1.22	1.23	1.32	C9-C5-C6	119.72	121.97	121.94	120.08
C4-N8	1.37	1.37	1.37	1.37	C6-N1-C10	120.62	122.01	119.83	122.21
C5-C9	1.49	1.51	1.50	1.50	N1-C2-O7	114.45	122.76	119.25	115.73

S1.1.2 Excited states at the FC point (GS minimum)

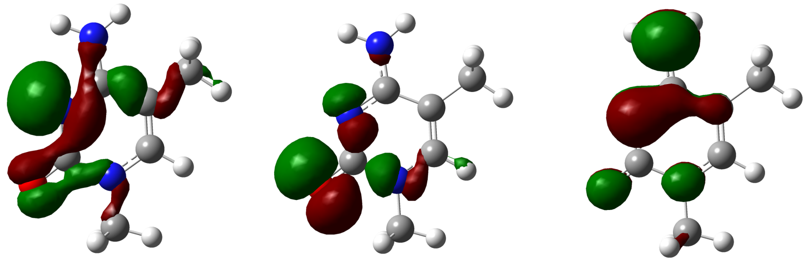

(a) n_N [HOMO-3] **(b)** n_O [HOMO-2] **(c)** π_1 [HOMO-1]

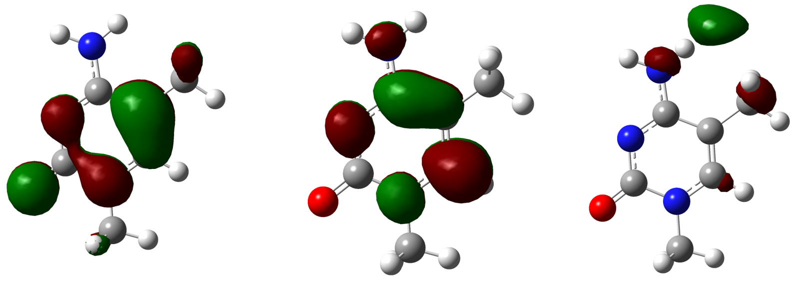

(d) π_H [HOMO] **(e)** π^*_L [LUMO] **(f)** $Ryd1$ [LUMO+1]

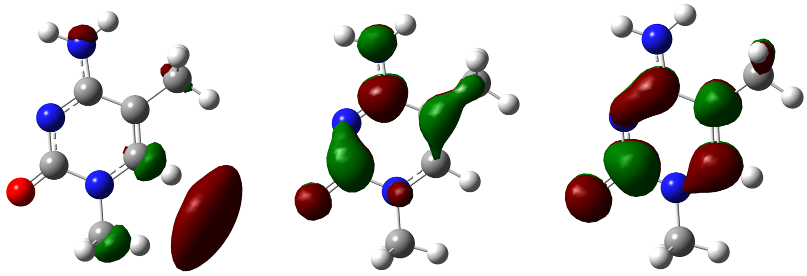

(g) $Ryd2$[LUMO+2] **(h)** π^*_3 [LUMO+5] **(i)** π^*_2 [LUMO+7]

Figure S1: Schematic drawing of the Kohn-Sham molecular orbitals of 1,5diMe-Cyt involved in the electronic transitions discussed in the present paper, computed at CAM-B3LYP/6-31+G(d,p) level of theory with isovalue 0.04.

1,5 di Methyl-Cytosine-Gas-CAM-FC

State	Transition energy(eV)	Osc. strength	Main contributions	Description	Orbital	DD
1	A' 4.8162	0.1039	37 - 38 0.68734 E(TD-HF)=-473.1880	π_H-π^*_L	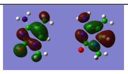	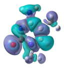
2	A'' 5.3277	0.0023	34 - 38 0.55221 35 - 38 0.37502	$n_N - \pi^*_L$ $n_O - \pi^*_L$	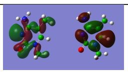 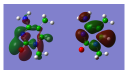	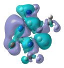
3	A'' 5.6774	0.0022	37 - 39 0.59502	π_H-$Ry1$	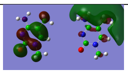	
4	A' 5.8535	0.1377	36 - 38 0.67233	π_1-π^*_L	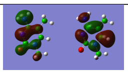	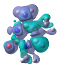
5	A'' 5.8704	0.0002	35 - 38 0.46700 34 - 38 -0.3352	$n_O - \pi^*_L$ $n_N - \pi^*_L$	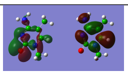 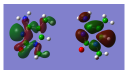	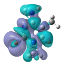
6	A'' 6.0811	0.0153	37 - 40 0.58396	π_H-$Ry2$	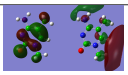	
7	A'' 6.1621	0.0002	35 - 45 0.46610 35 - 38 0.35164	$n_O - \pi^*_2$ $n_O - \pi^*_L$	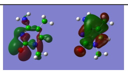 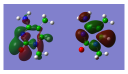	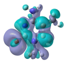

Figure S2: Excited states of 1,5diMe-Cyt at the ground-state minimum in the gas phase using CAM-B3LYP functional. We also report Kohn-Sham orbitals (left/right occupied/virtual, isovalue 0.02), and for some states a plot of the difference of the electronic density with respect to the ground state, where violet and cyan indicate respectively a depletion and an increase of the density.

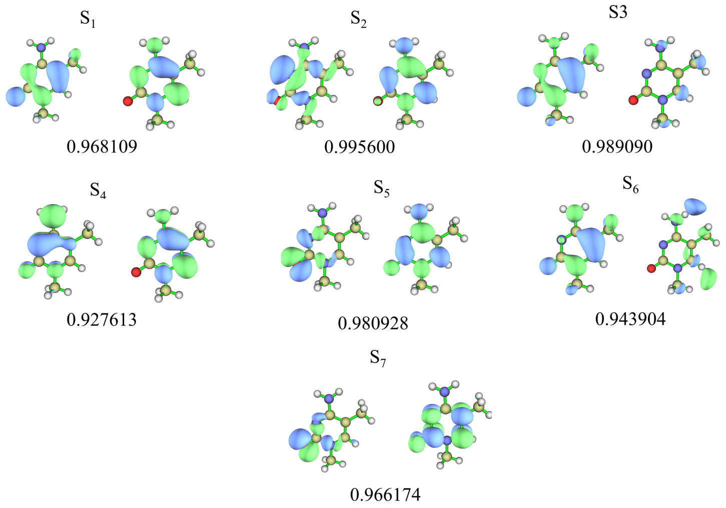

Figure S3: Natural transition orbitals (NTOs) of 1,5diMe-Cyt in gas phase at ground state geometry using CAM-B3LYP functional and an isovalue 0.04. The weight of each transition in the corresponding excited state is also reported.

S1.1.3 Excited states at the minimum of the first $\pi\pi^*$ state

1,5di-Methyl-Cytosine-Gas-CAM-Min of First Bright State

State	Transition energy(eV)	Osc. strength	Main contributions	Description	Orbital	DD
1	A' 4.4717	0.0736	37 - 38 0.69677 E(TD-HF=-473.200689109)	$\pi_H - \pi^*_L$	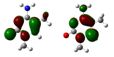	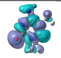
2	A'' 5.1709	0.0000	36 - 38 0.69803	n_O-π^*_L	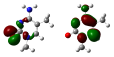	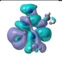
3	A'' 5.4386	0.0023	34 - 38 0.67184	$n_N - \pi^*_L$	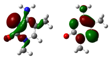	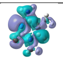
4	A' 5.6723	0.1797	35 - 38 0.68924	$\pi_1 - \pi^*_L$	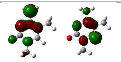	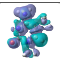
5	A'' 5.9335	0.0025	37 - 39 0.60762	$\pi_H - Ry1$	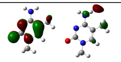	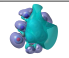
6	A'' 6.1802	0.0000	36 - 45 0.57098	$n_O - \pi^*_2$	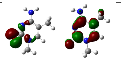	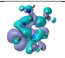
7	A'' 6.3423	0.0093	37 - 40 0.63803	$\pi_H - Ry2$	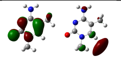	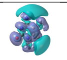

Figure S4: Excited states of 1,5diMe-Cyt in the gas phase at the minimum of the first $\pi\pi^*$ using CAM-B3LYP functional. We also report Kohn-Sham orbitals (left/right occupied/virtual, isovalue 0.02), and for some states a plot of the difference of the electronic density with respect to the ground state, where violet and cyan indicate respectively a depletion and an increase of the density.

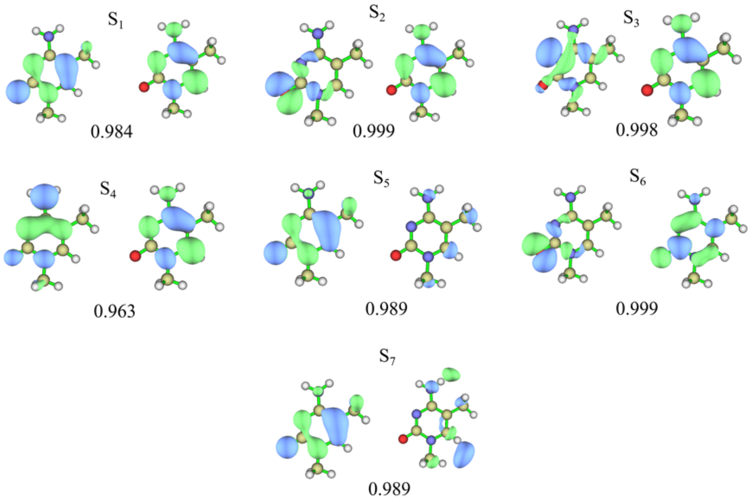

Figure S5: Natural transition orbitals (NTOs) of 1,5diMe-Cyt in the gas phase at the minimum of the first $\pi\pi^*$ state using CAM-B3LYP functional and an isovalue 0.04. The weight of each transition in the corresponding excited states is also reported.

S1.1.4 Excited states at the minimum of the first nπ^* state ($n_N\pi_L^*$)

1,5 di-Methyl-Cytosine-Gas-CAM-Min of First Dark State

State	Transition energy(eV)	Osc. strength	Main contributions	Description	Orbital	DD
1	A'' 4.6941	0.0013	36 - 38 0.68534 E(TD-HF=-473.1925)	$n_N - \pi_L^*$	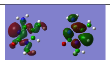	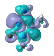
2	A' 5.2086	0.0796	37 - 38 0.69302	π_H-π_L^*	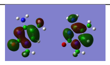	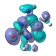
3	A' 6.1561	0.1771	35 - 38 0.67184	$\pi_1 - \pi_L^*$	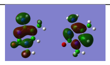	
4	A'' 6.1568	0.0000	34 - 38 0.68124	$n_O - \pi_L^*$	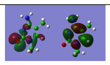	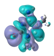
5	A'' 6.4826	0.0025	37 - 39 0.58787	$\pi_H - Ry1$	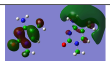	
6	A'' 6.6846	0.0011	36 - 45 0.53712	$n_N - \pi_2^*$	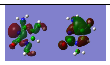	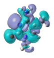
7	A'' 6.8522	0.0014	35 - 39 0.48554	$\pi_1 - Ry1$	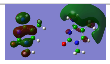	

Figure S6: Excited states of 1,5diMe-Cyt in the gas phase at the minimum of the first nπ^* state (n$_N\pi_L^*$) using CAM-B3LYP functional. We also report Kohn-Sham orbitals (left/right occupied/virtual, isovalue 0.02), and for some states a plot of the difference of the electronic density with respect to the ground state, where violet and cyan indicate respectively a depletion and an increase of the density.

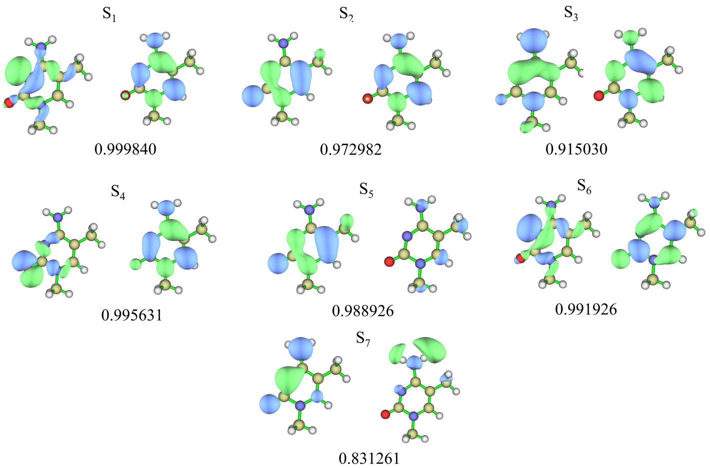

Figure S7: Natural transition orbitals (NTOs) of 1,5diMe-Cyt in gas phase at ground state geometry using CAM-B3LYP functional from the minimum of the first nπ^* and an isovalue 0.04. The weight of each transition in the corresponding excited states is also reported.

S1.1.5 Excited states at the minimum of the second nπ^* state ($n_O\pi^*_L$)

1,5 di-Methyl-Cytosine-Gas-CAM-Min of Second Dark State

State	Transition energy(eV)	Osc. strength	Main contributions	Description	Orbital	DD
1	A' 4.6699	0.0263	37 - 38 0.70139	π_H-π^*_L	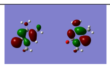	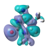
2	A'' 4.8185	0.0001	36 - 38 0.69788 E(TD-HF=-473.187944693)	n$_O\pi^*_L$	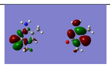	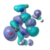
3	A'' 5.9475	0.0018	34 - 38 0.68673	n$_N\pi^*_L$	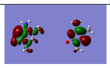	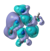
4	A' 6.2043	0.2110	35 - 38 0.68682	π_1-π^*_L	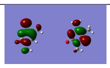	
5	A'' 6.3196	0.0000	36 - 45 0.56456	n$_O\pi^*_2$	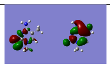	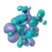
6	A'' 6.5088	0.0059	37 - 39 0.59181	π_H-$Ry1$	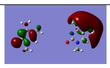	
7	A'' 6.8742	0.0023	37 - 40 0.62324	π_H-$Ry2$	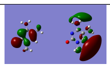	

Figure S8: Excited states of 1,5diMe-Cyt in the gas phase at the minimum of the second nπ^* state (n$_O\pi^*_L$) using CAM-B3LYP functional. We also report Kohn-Sham orbitals (left/right occupied/virtual, isovalue 0.02), and for some states a plot of the difference of the electronic density with respect to the ground state, where violet and cyan indicate respectively a depletion and an increase of the density.

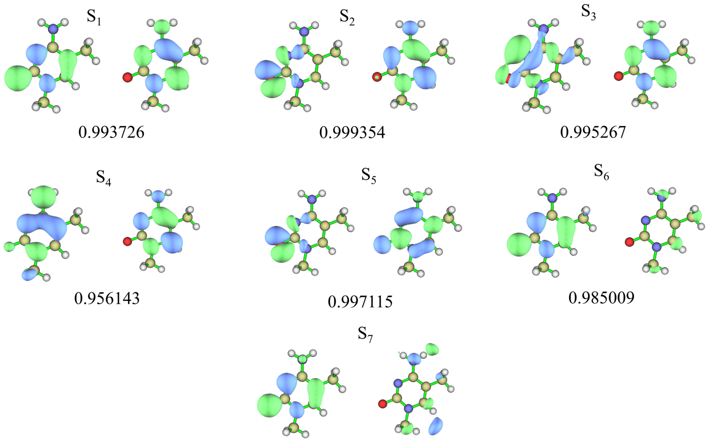

Figure S9: Natural transition orbitals (NTOs) of 1,5diMe-Cyt in gas phase at ground state geometry using CAM-B3LYP functional from the minimum of second nπ^* and an isovalue 0.04. The weight of each transition in the corresponding state is also reported.

S1.2 PBE0

S1.2.1 Optimized geometries (C_S symmetry) of the ground and excited states and normal modes with imaginary frequencies

The structures we report in the following of $\pi_H\pi_L^*$ and $n_N\pi_L^*$ correspond to minima on the lowest adiabatic PES S1 (the former more stable than the latter). Excited state energies at the different stationary points are reported in section S1.2.3.

Table S7: Cartesian coordinates of 1,5diMe-Cyt at the minimum of GS. PBE0/6-31+G(d,p) calculations in gas phase.

Cytosine-Minimum of GS			
C	0.000000	1.302687	0.000000
C	-1.244793	-0.769167	0.000000
C	1.083228	-0.787151	0.000000
C	1.193714	0.648350	0.000000
N	-1.184946	0.650363	0.000000
N	-0.059058	-1.439958	0.000000
N	2.213138	-1.535613	0.000000
O	-2.347340	-1.298501	0.000000
H	-0.052641	2.388456	0.000000
H	3.130302	-1.127475	0.000000
H	2.111897	-2.537828	0.000000
C	2.511530	1.359685	0.000000
H	3.110842	1.114332	0.886491
H	3.110842	1.114332	-0.886491
H	2.366651	2.443814	0.000000
C	-2.452397	1.357684	0.000000
H	-3.034833	1.081805	-0.882446
H	-3.034833	1.081805	0.882446
H	-2.261146	2.432684	0.000000

Table S8: Cartesian coordinates of 1,5diMe-Cyt at the minimum of the first $\pi\pi^*$ state (character $\pi_H\pi_L^*$). PBE0/6-31+G(d,p) calculations in gas phase.

Cytosine-Minimum of first $\pi\pi^*$ state			
C	0.000000	1.351484	0.000000
C	-1.184034	-0.719119	0.000000
C	1.122979	-0.764213	0.000000
C	1.207756	0.613794	0.000000
N	-1.207261	0.655064	0.000000
N	-0.098237	-1.444581	0.000000
N	2.196428	-1.603064	0.000000
O	-2.354975	-1.278781	0.000000
H	-0.046093	2.430256	0.000000
H	3.142042	-1.268126	0.000000
H	2.018058	-2.592589	0.000000
C	2.522506	1.325331	0.000000
H	3.119577	1.068488	0.885513
H	3.119577	1.068488	-0.885513
H	2.386129	2.409764	0.000000
C	-2.466105	1.380891	0.000000
H	-3.057138	1.142707	-0.887308
H	-3.057138	1.142707	0.887308
H	-2.240333	2.447619	0.000000

Table S9: Cartesian coordinates of 1,5diMe-Cyt at the minimum of the first nπ^* state (character $n_N\pi_L^*$). PBE0/6-31+G(d,p) calculations in gas phase.

Cytosine-Minimum of first nπ^* state			
C	-0.073182	1.316314	0.000000
C	-1.263996	-0.830538	0.000000
C	1.229983	-0.686699	0.000000
C	1.181935	0.700405	0.000000
N	-1.264492	0.570764	0.000000
N	0.000000	-1.293304	0.000000
N	2.340153	-1.480856	0.000000
O	-2.290411	-1.490203	0.000000
H	-0.188403	2.390892	0.000000
H	3.253754	-1.067876	0.000000
H	2.257988	-2.480585	0.000000
C	2.455744	1.496014	0.000000
H	3.067962	1.295221	0.888358
H	3.067962	1.295221	-0.888358
H	2.226163	2.564649	0.000000
C	-2.563946	1.206433	0.000000
H	-3.140511	0.924704	-0.886426
H	-3.140511	0.924704	0.886426
H	-2.409960	2.286887	0.000000

Table S10: Normal modes and imaginary frequencies of 1,5diMe-Cyt calculated at different stationary points (FC is the ground state minimum, for other geometries the character of the state with vanishing gradient is given), computed at PBE0/6-31G+(d,p) level.

Geometries	mode	ω (cm^{-1})	description
FC	1	i150	NH$_2$ pyramidalization bending out-of plane
$\pi_H\pi_L^*$	1	i1029.84	Methyl rotation and ring out of plane
	2	i362.37	NH$_2$ pyramidalization bending out-of plane
	3	i162.55	Methyl rotation and H(C$_6$) out of plane
n$_N\pi_H^*$	1	i490.03	NH$_2$ pyramidalization bending out-of plane
	2	i177.37	Methyl rotation and ring out of plane
	3	i150.00	Methyl rotation and ring out of plane
	4	i12.74	Methyl rotation and ring out of plane

S1.2.2 Excited States at the FC point (GS minimum)

State	Transition energy(eV)	Osc. strength	Main contributions	Description	Orbital	DD
1	A' 4.6286	0.0821	37 - 38 0.69355 E(TD-HF)=-472.8867	π_H-π^*_L	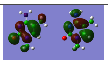	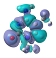
2	A'' 5.0192	0.0013	35 - 38 0.60259 34 - 38 0.35747	$n_O - \pi^*_L$ $n_N - \pi^*_L$	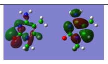 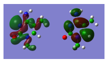	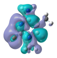
3	A'' 5.3112	0.0010	34 - 38 0.59827 35 - 38 -0.36020	$n_N - \pi^*_L$ $n_O - \pi^*_L$	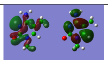 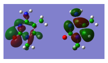	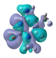
4	A'' 5.3821	0.0002	37 - 39 0.68292	π_H-$Ry1$	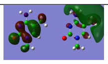	
5	A' 5.5169	0.1119	36 - 38 0.67656	π_1-π^*_L	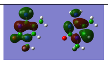	
6	A'' 5.6975	0.0088	37 - 40 0.68541	π_H-$Ry2$	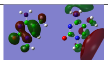	
7	A'' 5.9043	0.0002	35 - 41 0.67240	$n_O - \pi^*_2$	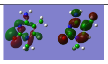	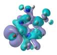

Figure S10: Excited states of 1,5diMe-Cyt in gas phase at the minimum of the ground state geometry using PBE0 functional. We also report Kohn-Sham orbitals (left/right occupied/virtual, isovalue 0.02), and for some states a plot of the difference of the electronic density with respect to the ground state, where violet and cyan indicate respectively a depletion and an increase of the density.

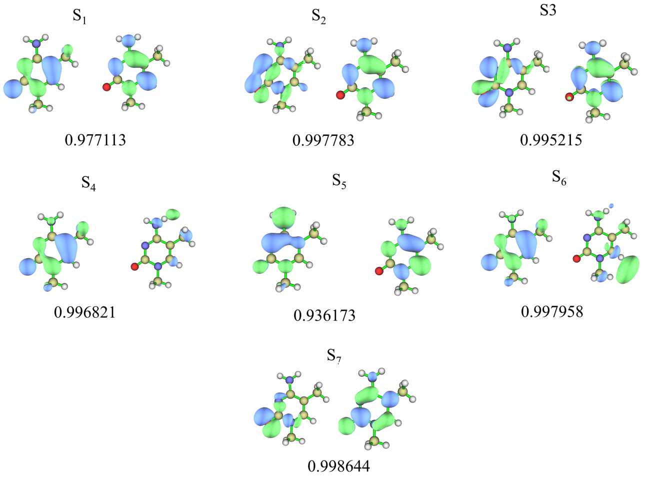

Figure S11: Natural transition orbitals (NTOs) of 1,5diMe-Cyt in gas phase at ground state geometry using PBE0 functional and an isovalue 0.04. The weight of each transition in the corresponding excited state is also reported.

S1.2.3 Excited states in the minima of first bright and dark states

Table S11: Energies (E^a) of the adiabatic states of 1,5 dimethyl-cytosine in the minima of the first $\pi\pi^*$ and first $n\pi^*$ states and their electronic characters. PBE0/6-31+G(d,p) calculations in gas phase.

PBE0			
First $\pi\pi^*$		First $n\pi^*$	
E^a	character	E^a	character
4.18	$\pi_H\pi_L^*$	4.49	$n_N\pi_L^*$
4.20	$n_O\pi_L^*$	4.96	$\pi_H\pi_L^*$
5.37	$n_N\pi_L^*$	5.45	$n_O\pi_L^*$
5.55	$\pi_1\pi_L^*$	5.83	$\pi_1\pi_L^*$
5.75	$\pi_H Ry_\sigma 1$	6.09	$\pi_H Ry_\sigma 1$
5.87	$n_O\pi_2^*$	6.40	$\pi_H Ry_\sigma 2$
6.07	$\pi_1 Ry_\sigma 1$	6.42	$n_N\pi_2^*$

Optimization of a minimum with $n_O\pi_L^*$ character failed. However in Section 2.3.1 (Figure S16) we report scans of the TD-DFT energies along a collective coordinates leading from the GS minimum to the minima of the first four diabatic electronic states computed according to the LVC model. In the scan along the coordinate connecting the GS minimum and the minimum of the $n_0\pi_L^*$-$n_N\pi_L^*$ a degeneracy point is found between the S1 and S2 PES at both LVC and TD-DFT levels. We checked that at that point the S1 adiabatic state switches character from $\pi_H\pi_L^*$ to $n_0\pi_L^*$. This proves that there is a region of the coordinate state where the S1 adiabatic state has a $n_0\pi_L^*$ character. Unfortunately, even starting a re-optimization of the $n_0\pi_L^*$ state from the local minimum on S1 individuated along this scan, the procedure fails probably for the very strong couplings with other states. Notwithstanding this, we found a geometry where S1 has $n_0\pi_L^*$ character and an energy 4.13 eV with respect to the GS in its minimum. Therefore, such point is 0.05 eV more stable than the $\pi_H\pi_L^*$ minimum located on S1 (Table S11) supporting the fact that a global minimum on S1 should have $n_0\pi_L^*$ character.

S2 Linear Vibronic Coupling Model

We consider a model Hamiltonian in the n dimensional diabatic basis $|\mathbf{d}^{(r)}\rangle$ ($|\mathbf{d}^{(r)}\rangle = (|d_1\rangle, |d_2\rangle, \cdots, |d_n\rangle)$), using ground state (S$_0$) dimensionless normal coordinates $\mathbf{q}$ (column vector), and conjugated momenta $\mathbf{p}$.

$$H = \sum_i \left(K + V_{ii}^{dia}(\mathbf{q})\right) |d_i\rangle\langle d_i| + \sum_{i,j>i} V_{ij}^{dia}(\mathbf{q})(|d_i\rangle\langle d_j| + |d_j\rangle\langle d_i|) \tag{1}$$

K is the kinetic term and V_{ii}^{dia} is diagonal potential energy surfaces (PES). In our LVC Hamiltonian, K and V_{ii}^{dia} are written in harmonic approximation within the assumption that excited diabatic states have the same frequencies and normal modes of S$_0$. Moreover, the couplings among the diabatic states, $V_{ij}^{dia}(\mathbf{q})$ ($i \neq j$), are taken as linear functions of $\mathbf{q}$

$$\begin{aligned} K &= \frac{1}{2}\mathbf{p}^T \boldsymbol{\Omega} \mathbf{p} && (2) \\ V_{ii}^{dia}(\mathbf{q}) &= E_i^0 + \boldsymbol{\lambda}_{ii}^T \mathbf{q} + \frac{1}{2}\mathbf{q}^T \boldsymbol{\Omega} \mathbf{q}, && (3) \\ V_{ij}^{dia}(\mathbf{q}) &= \boldsymbol{\lambda}_{ij}^T \mathbf{q}. && (4) \end{aligned}$$

In Eqs. 2-4, the diagonal matrix $\boldsymbol{\Omega}$ has elements corresponding to the frequencies of the normal modes in S$_0$, whereas the superscript T indicates that the transpose is taken. The time-dependent vibronic wavepacket is written as $|\Psi(\mathbf{q}, t)\rangle = \sum_i |d_i\rangle|\Psi_i(\mathbf{q}, t)\rangle$, and it is numerically propagates with ML-MCTDH method.

In the following two sections we report the LVC parameters obtained at CAM-B3LYP and PBE0 level adopting as reference geometry the ground state minimum (FC point). For the sake of brevity, inter-state couplings are only reported for the two lowest $\pi\pi^*$ and nπ^* states.

S2.1 Parametrization of LVC at FC point with CAM-B3LYP

Table S12: The intra-state couplings (i.e. the components of the energy gradient) of the diabatic states of 1,5diMe-Cyt according to the LVC model parametrized at FC position. Data in eV for CAM-B3LYP/6-31+G(d,p) calculations in gas phase. Largest couplings are highlighted in bold.

Mode	Frequency	$\pi_H\pi_L^*$	n$_N\pi_L^*$	$\pi_H Ry_\sigma 1$	$\pi_1\pi_L^*$	n$_O\pi_L^*$	$\pi_H Ry_\sigma 2$	n$_O\pi_2^*$
7	286.7	0.002	0.001	-0.010	0.007	0.005	-0.010	0.006
9	336.8	0.012	0.015	-0.005	0.036	0.026	-0.003	0.015
10	383.4	-0.000	0.032	-0.015	0.042	0.043	-0.011	-0.014
12	469.5	0.051	0.014	0.044	-0.039	**0.075**	0.030	0.025
13	547.5	0.033	**-0.122**	0.034	0.012	0.004	0.032	0.006
15	627.8	-0.035	**-0.077**	-0.003	-0.019	0.007	-0.010	-0.008
16	701.1	0.045	-0.132	0.025	0.018	-0.022	0.031	0.034
19	787.7	-0.046	**-0.098**	-0.002	-0.038	-0.005	-0.020	0.022
20	870.9	0.032	0.024	0.007	0.051	-0.048	0.010	-0.033
22	1034.0	0.050	**0.078**	-0.012	0.051	0.035	-0.014	0.038
24	1079.2	-0.013	**0.077**	-0.011	-0.018	0.037	-0.014	-0.026
25	1096.5	0.011	0.0008	0.068	-0.057	-0.038	0.068	-0.060
27	1186.9	-0.041	-0.039	-0.018	0.004	-0.024	-0.016	0.045
28	1248.0	**0.071**	0.058	0.028	-0.025	**0.079**	0.049	-0.087
29	1316.9	**0.078**	0.019	0.034	0.029	**0.082**	0.045	-0.103
30	1359.8	0.057	-0.001	0.068	0.004	-0.003	**0.089**	0.050
31	1427.1	0.049	0.026	0.033	-0.012	0.053	0.039	-0.061
32	1443.7	0.023	0.010	-0.001	0.004	0.028	0.013	-0.031
33	1475.9	-0.060	-0.012	-0.068	-0.022	-0.033	**-0.071**	-0.030
36	1497.7	-0.043	-0.006	0.051	**-0.083**	-0.003	0.020	-0.039
37	1523.3	0.021	0.010	-0.039	0.054	0.013	-0.038	0.018
38	1537.3	-0.018	-0.025	-0.052	0.002	-0.024	-0.056	-0.019
39	1592.4	**-0.248**	**-0.167**	-0.012	**-0.308**	**-0.172**	**0.013**	**-0.149**
40	1649.3	0.038	0.012	0.061	-0.004	0.050	**0.077**	**0.077**
41	1750.3	0.051	**-0.153**	**0.093**	-0.021	-0.006	0.062	**0.209**
42	1790.4	**-0.090**	0.021	0.063	-0.051	**-0.519**	0.062	**-0.331**
43	3047.0	-0.007	0.002	-0.018	-0.011	0.000	-0.003	-0.016
44	3087.8	-0.004	-0.0024	0.006	-0.014	-0.020	-0.001	-0.005
46	3143.2	0.001	-0.001	0.003	0.004	-0.003	0.007	0.002
48	3180.0	0.005	0.002	0.008	0.009	0.021	-0.003	0.012
49	3219.8	0.038	0.029	0.018	0.037	0.018	-0.039	0.020
50	3644.6	-0.016	-0.027	0.024	0.037	-0.028	**0.079**	-0.002
51	3787.9	0.002	-0.003	-0.016	-0.008	0.001	-0.034	-0.002

Table S13: The inter-state couplings (eV) along total symmetric modes between the two lowest $\pi\pi^*$ or nπ^* states of 1,5diMe-Cyt according to the LVC model parametrized at FC position. CAM-B3LYP/6-31+G(d,p) calculations in gas phase. Largest couplings are highlighted in bold.

Mode	$< \pi_H\pi_L^*\|H\|\pi_1\pi_L^* >$	$< n_N\pi_L^*\|H\|n_O\pi_L^* >$
7	0.001	0.003
9	0.003	0.001
10	0.024	**-0.032**
12	0.024	-0.020
13	-0.014	**0.032**
15	-0.005	-0.021
16	-0.021	**0.074**
19	**0.042**	0.027
20	-0.018	**0.030**
22	0.001	-0.021
24	-0.008	0.001
25	**-0.045**	-0.002
27	0.014	0.003
28	**-0.041**	-0.026
29	**-0.035**	0.016
30	-0.003	-0.004
31	**-0.034**	0.005
32	-0.019	-0.001
33	0.013	0.006
36	-0.015	**-0.036**
37	0.008	0.007
38	-0.015	**0.046**
39	**-0.088**	0.009
40	0.013	-0.025
41	-0.017	0.021
42	**-0.055**	**-0.056**
43	-0.004	-0.000
44	0.003	-0.002
46	0.001	0.001
48	-0.001	0.003
49	-0.001	-0.001
50	-0.001	-0.000
51	-0.002	0.001

Table S14: The inter-state couplings (eV) along non-total symmetric modes involving the first two $\pi\pi$ and nπ states (eV) of 1,5diMe-Cyt according to the LVC model parametrized at FC position. CAM-B3LYP/6-31+G(d,p) calculations in gas phase. Largest couplings are highlighted in bold.

Mode	Frequency	$< \pi_H\pi_L^*\|H\|\mathrm{n}_N\pi_L^* >$	$< \pi_H\pi_L^*\|H\|\mathrm{n}_O\pi_L^* >$	$< n_N\pi_L^*\|H\|\pi_1\pi_L^* >$	$< n_O\pi_L^*\|H\|\pi_1\pi_L^* >$
2	80.7	0.009	**-0.038**	0.011	**0.031**
3	116.1	**0.033**	0.015	0.003	-0.029
4	163.0	-0.021	0.014	-0.026	0.015
5	208.1	-0.018	0.004	-0.011	0.005
6	235.8	0.024	**-0.035**	**0.049**	**-0.033**
8	297.7	**-0.042**	-0.008	**0.059**	0.005
11	427.9	-0.018	**-0.058**	0.009	0.003
14	561.8	0.006	0.005	0.006	0.024
17	756.0	**-0.046**	0.022	0.019	**0.037**
18	787.6	-0.029	0.016	**-0.051**	0.011
21	941.6	-0.029	-0.012	0.003	0.001
23	1078.2	0.019	-0.001	-0.012	0.006
26	1159.7	-0.020	-0.014	0.011	0.010
34	1479.7	-0.012	-0.010	0.009	0.005
35	1496.8	0.008	-0.006	-0.003	0.003
45	3100.6	0.000	0.000	-0.000	-0.000
47	3166.8	0.003	0.007	-0.003	-0.009

Table S15: The energies of all diabatic states in all the diabatic-state minima of 1,5diMe-Cyt according to a LVC Hamiltonian parametrized at the ground state minimum. CAM-B3LYP/6-31+G(d,p) calculations in gas phase.

IN MIN STATE	$\pi_H\pi_L^*$	n$_N\pi_L^*$	$\pi_H Ry_\sigma 1$	$\pi_1\pi_L^*$	n$_O\pi_L^*$	$\pi_H Ry_\sigma 2$	n$_O\pi_2^*$
S_0	4.816	5.328	5.677	5.854	5.870	6.081	6.162
$\pi_H\pi_L^*$	4.478	5.432	5.843	5.706	5.602	6.254	6.153
n$_N\pi_L^*$	5.092	4.818	6.310	6.024	6.101	6.689	6.855
$\pi_H Ry_\sigma 1$	4.789	5.596	5.532	6.091	6.077	5.948	6.311
$\pi_1\pi_L^*$	4.709	5.368	6.148	5.475	5.846	6.548	6.211
n$_O\pi_L^*$	5.062	5.901	6.591	6.303	5.018	7.011	6.160
$\pi_H Ry_\sigma 2$	4.807	5.582	5.555	6.098	6.104	5.925	6.383
n$_O\pi_2^*$	5.028	6.070	6.240	6.083	5.575	6.705	5.603

Table S16: Norm (eV) of the energy gradients of the diabatic states and of the coupling vectors between the diabatic states for 1,5diMe-Cyt according to the LVC model parametrized at FC position. CAM-B3LYP/6-31+G(d,p) calculations in gas phase

STATE	$\pi_H\pi_L^*$	n$_N\pi_L^*$	$\pi_H Ry_\sigma 1$	$\pi_1\pi_L^*$	n$_O\pi_L^*$	$\pi_H Ry_\sigma 2$	n$_O\pi_2^*$
$\pi_H\pi_L^*$	0.337						
n$_N\pi_L^*$	0.098	0.350					
$\pi_H Ry_\sigma 1$	0.099	0.003	0.215				
$\pi_1\pi_L^*$	0.150	0.134	0.035	0.359			
n$_O\pi_L^*$	0.089	0.138	0.002	0.078	0.581		
$\pi_H Ry_\sigma 2$	0.085	0.006	0.076	0.046	0.009	0.235	
n$_O\pi_2^*$	0.055	0.118	0.006	0.046	0.271	0.007	0.472

S2.1.1 Additional relevant normal modes

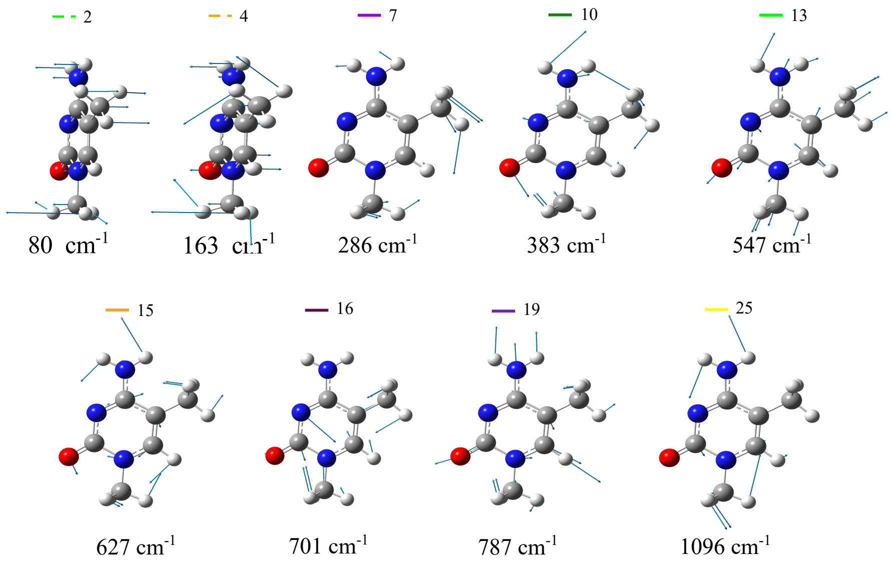

Figure S12: A' (solid line) and A'' (dash line) normal modes of 1,5diMe-Cyt more relevant for the dynamics computed at CAM-B3LYP level of theory beside those given in the Figure 2 of the main text. PBE0 modes are very similar.

S2.2 Parametrization of LVC at FC point with PBE0

Table S17: The intra-state couplings (i.e. the components of the energy gradient) of the diabatic states of 1,5diMe-Cyt according to the LVC model parametrized at FC position. Data in eV for PBE0/6-31+G(d,p) calculations in gas phase. Largest couplings are highlighted in bold.

Mode	Frequency	$\pi_H\pi_L^*$	$n_O\pi_L^*$+n$_N\pi_L^*$	$n_O\pi_L^*$-n$_N\pi_L^*$	$\pi_H Ry_\sigma 1$	$\pi_1\pi_L^*$	$\pi_H Ry_\sigma 2$	$n_O\pi_2^*$
7	282.4	0.002	0.009	0.009	-0.008	0.009	-0.011	-0.005
9	333.2	0.013	0.025	0.033	-0.006	0.039	-0.011	0.004
10	379.4	0.004	0.004	**0.074**	-0.014	0.044	-0.002	-0.013
12	466.8	0.051	0.006	**0.079**	0.045	-0.037	0.055	0.023
13	545.3	0.033	-0.056	-0.034	0.028	0.019	0.033	-0.020
15	623.3	-0.034	**-0.079**	0.012	-0.006	-0.010	-0.013	-0.005
16	699.7	0.040	-0.041	**-0.112**	0.024	0.024	0.026	0.028
19	784.3	-0.039	-0.030	-0.014	-0.002	-0.042	-0.013	-0.012
20	869.2	0.013	0.024	-0.069	-0.002	0.036	-0.008	-0.045
22	1023.2	0.045	**0.070**	**0.089**	-0.021	0.067	-0.011	0.018
24	1076.9	0.001	-0.061	-0.035	-0.003	0.019	0.007	0.000
25	1089.8	-0.019	-0.042	-0.066	0.052	-0.059	0.047	-0.025
27	1181.5	-0.028	-0.014	-0.013	-0.022	0.013	-0.010	0.038
28	1250.4	0.048	0.026	**0.093**	0.029	-0.037	0.036	**-0.078**
29	1316.6	0.053	0.008	0.032	0.022	0.001	0.024	**-0.084**
30	1350.3	0.041	0.002	0.004	0.061	0.004	**0.079**	0.024
31	1416.9	0.033	0.024	0.026	0.031	-0.009	0.026	-0.029
32	1435.6	0.041	0.023	0.033	0.019	0.013	-0.000	-0.022
33	1462.4	-0.063	-0.029	-0.045	-0.064	-0.033	-0.063	-0.013
36	1490.5	-0.033	-0.043	-0.000	0.040	**-0.085**	0.012	-0.001
37	1512.7	0.017	0.023	0.013	-0.048	0.058	-0.039	-0.004
38	1534.4	-0.013	0.019	-0.063	**-0.080**	0.039	-0.060	-0.013
39	1585.9	**-0.255**	**-0.24**	**-0.303**	-0.022	**-0.300**	-0.010	0.037
40	1646.8	0.040	0.007	**0.072**	**0.086**	-0.014	**0.085**	0.068
41	1741.1	0.023	**-0.098**	**-0.074**	0.063	0.024	0.052	**0.184**
42	1793.3	**-0.157**	**-0.130**	**-0.345**	0.012	-0.035	0.018	**-0.419**
43	3038.9	-0.008	-0.001	-0.002	-0.027	-0.017	0.002	-0.018
44	3080.4	-0.005	-0.005	-0.011	0.007	-0.015	-0.010	-0.010
46	3145.9	0.001	0.000	-0.003	-0.009	0.006	0.007	0.004
48	3181.4	0.006	0.008	0.013	0.006	0.009	-0.011	0.014
49	3213.9	0.037	0.036	0.036	0.017	0.042	-0.056	0.005
50	3656.2	-0.015	-0.023	-0.023	0.056	0.037	0.059	-0.010
51	3804.3	0.001	-0.002	-0.002	-0.039	-0.009	-0.019	0.000

A detailed comparison of the LVC parameters obtained with PBE0 and CAM-B3LYP is not easy because the S$_0$ normal modes are in principle not identical according to the two functionals. Moreover, the diabatic states are different for each functionals (especially the nπ^* states), it is not possible to establish a one-to-one correspondence. Finally, the number of parameters is very large: we have 7 electronic states and 51 coordinates, so each LVC model comprises 7 vertical excitations, 51 normal frequencies, 7×51 intra-state couplings and $\frac{7(7-1)}{2}\times 51$ interstate couplings for a total of 1486 parameters. However some general considerations are possible since, at least, S_0 normal modes (and frequencies) obtained with the functionals are actually very similar. However, please recall that there is no guarantee that their sign is the same, so that possible apparent inversions of the sign of the coupling coefficients $\lambda_{ii,k}$ and $\lambda_{ij,k}$, if k is the normal mode, might occur. The most relevant modes are sketched in Figure 2 in the min text and in Figure S12 of this ESI.

A remarkable difference between the PBE0 and CAM-B3LYP concerns the vertical transitions energies, i.e. the E_i^0 parameters in Eq.3 which, by construction are identical to the E^a_{FC} data reported in Table 1 of the main manuscript .

Concerning the intra-state couplings along the total symmetric modes, there are many analogies among the two sets of parameters. As expected, Rydberg states exhibit small couplings (i.e. small displacements). They have little impact on dynamics studied in this work (see also Figure S22 and related comments). The PBE0 and CAM-B3LYP values for the two first and the second $\pi\pi^*$ states are similar. In both cases $\pi_H\pi_L^*$ has the largest component along modes 39 (collective CC

Table S18: The inter-state couplings (eV) along non-total symmetric modes involving the two $\pi\pi$ and nπ states of 1,5diMe-Cyt according to the LVC model parametrized at FC position. PBE0/6-31+G(d,p) calculations in gas phase. Largest couplings are highlighted in bold

Mode	Frequency	$< \pi_H\pi_L^*\|H\|$ $n_O\pi_L^*$+n$_N\pi_L^* >$	$< \pi_H\pi_L^*\|H\|$ $n_O\pi_L^*$-n$_N\pi_L^* >$	$< \pi_1\pi_L^*\|H\|$ $n_O\pi_L^*$+n$_N\pi_L^* >$	$< \pi_1\pi_L^*\|H\|$ $n_O\pi_L^*$-n$_N\pi_L^* >$
2	79.7	-0.010	**0.044**	0.025	**-0.032**
3	111.2	**0.040**	-0.003	-0.014	0.028
4	161.5	0.012	0.028	0.012	0.029
5	207.9	-0.014	-0.012	-0.005	-0.008
6	233.2	0.009	**0.043**	0.023	**0.051**
8	293.5	**-0.037**	-0.006	**0.057**	0.020
11	421.5	**-0.041**	**0.042**	0.013	0.004
14	560.8	0.006	0.000	0.017	-0.022
17	744.4	-0.029	**-0.044**	**0.031**	**-0.032**
18	778.6	-0.021	-0.015	**-0.038**	-0.029
21	922.7	-0.028	-0.001	0.005	0.001
23	1062.7	0.015	0.008	-0.009	-0.012
26	1148.1	-0.025	0.006	0.015	-0.004
34	1466.8	-0.018	0.004	0.011	0.001
35	1484.2	0.005	0.010	-0.002	-0.005
45	3098.7	0.000	-0.001	-0.001	-0.001
47	3164.4	0.007	-0.007	-0.007	0.008

stretching), but also an appreciable contribution along mode 42 (CO stretching), whereas for $\pi_1\pi_L^*$, the contribution of mode 39 is by far dominant. nπ^* intra-state

Table S19: The inter-state couplings (eV) along total symmetric modes between the two lowest $\pi\pi^*$ or nπ^* states of 1,5diMe-Cyt according to the LVC model parametrized at FC position. PBE0/6-31+G(d,p) calculations in gas phase.

Mode	Frequency	$<\pi_H\pi_L^*\|H\|\pi_1\pi_L^*>$	$< n_O\pi_L^* + \mathrm{n}_N\pi_L^*\|H\|\ n_O\pi_L^* - \mathrm{n}_N\pi_L^* >$
7	282.4	0.002	-0.005
9	333.2	0.005	-0.013
10	379.4	0.027	0.016
12	466.8	0.016	-0.009
13	545.3	-0.012	-0.080
15	623.3	-0.002	-0.014
16	699.7	-0.020	**-0.091**
19	784.3	**0.047**	**-0.075**
20	869.2	-0.011	0.021
22	1023.2	0.008	0.024
24	1076.9	0.010	-0.024
25	1089.8	**-0.043**	**0.039**
27	1181.5	0.013	-0.028
28	1250.4	**-0.035**	0.009
29	1316.6	**-0.037**	-0.017
30	1350.3	-0.005	0.003
31	1416.9	-0.021	-0.005
32	1435.6	-0.026	-0.010
33	1462.4	0.014	0.016
36	1490.5	-0.019	0.024
37	1512.7	0.013	-0.010
38	1534.4	-0.011	-0.026
39	1585.9	**-0.099**	**0.072**
40	1646.8	0.013	-0.006
41	1741.1	-0.017	**-0.048**
42	1793.3	**-0.070**	**0.259**
43	3038.9	-0.003	0.002
44	3080.4	0.003	0.005
46	3145.9	0.001	0.001
48	3181.4	-0.001	-0.008
49	3213.9	0.001	-0.002
50	3656.2	0.002	-0.002
51	3804.3	-0.003	-0.001

Table S20: Norm (eV) of the energy gradients of the diabatic potentials and of the coupling vectors between the diabatic states for 1,5diMe-Cyt according to the LVC model parametrized at FC position. PBE0/6-31+G(d,p) calculations in gas phase

STATE	$\pi_H\pi_L^*$	n$_O\pi_L^*$+n$_N\pi_L^*$	n$_O\pi_L^*$-n$_N\pi_L^*$	$\pi_H Ry_\sigma 1$	$\pi_1\pi_L^*$	$\pi_H Ry_\sigma 2$	n$_O\pi_2^*$
$\pi_H\pi_L^*$	0.347						
n$_O\pi_L^*$+n$_N\pi_L^*$	0.092	0.344					
n$_O\pi_L^*$-n$_N\pi_L^*$	0.095	0.319	0.535				
$\pi_H Ry_\sigma 1$	0.084	0.014	0.021	0.214			
$\pi_1\pi_L^*$	0.160	0.118	0.092	0.032	0.358		
$\pi_H Ry_\sigma 2$	0.089	0.003	0.005	0.092	0.021	0.209	
n$_O\pi_2^*$	0.020	0.174	0.129	0.006	0.017	0.007	0.488

Table S21: The energies of all diabatic states in all the diabatic-state minima of 1,5diMe-Cyt according to a LVC Hamiltonian parametrized at the minimum of the ground state. PBE0/6-31+G(d,p) calculations in gas phase.

IN MIN STATE	$\pi_H\pi_L^*$	$\mathrm{n}_O\pi_L^*$+$\mathrm{n}_N\pi_L^*$	$\mathrm{n}_O\pi_L^*$-$\mathrm{n}_N\pi_L^*$	$\pi_H Ry_\sigma 1$	$\pi_1\pi_L^*$	$\pi_H Ry_\sigma 2$	$\mathrm{n}_O\pi_2^*$
S_0	4.629	5.019	5.311	5.382	5.517	5.697	5.904
$\pi_H\pi_L^*$	4.286	4.867	4.880	5.569	5.362	5.890	5.990
$\mathrm{n}_O\pi_L^*$+$\mathrm{n}_N\pi_L^*$	4.496	4.657	4.843	5.805	5.388	6.133	6.152
$\mathrm{n}_O\pi_L^*$-$\mathrm{n}_N\pi_L^*$	4.720	5.055	4.446	6.202	5.835	6.524	6.242
$\pi_H Ry_\sigma 1$	4.610	5.218	5.403	5.245	5.726	5.580	5.995
$\pi_1\pi_L^*$	4.516	4.914	5.149	5.839	5.132	6.156	6.254
$\pi_H Ry_\sigma 2$	4.616	5.231	5.410	5.265	5.729	5.559	6.007
$\mathrm{n}_O\pi_2^*$	4.941	5.475	5.353	5.905	6.051	6.231	5.335

couplings involve the modes 39-42, but at variance with what happens for $\pi\pi^*$, they exhibit also some significant contributions along lower-frequency modes, like modes 13 , 15 and others. Although, for these states many similarities are found between PBE0 and CAM-B3LYP parameters, some remarkable differences emerge since the character of the states is different for the two functionals. In particular, as expected, mode 42 (the CO stretching) contributes more to the intra-state couplings of the states with a more pronounced $\mathrm{n}_O\pi_L^*$ character, so much that its value can be taken as an additional diagnostic of the "character" of the state. A remarkable difference is seen on the inter-state couplings along total-symmetric modes. The coupling of the two lowest $\mathrm{n}\pi_L^*$ states is strongly localized on mode 42 and is larger for PBE0 where the $\mathrm{n}_N\pi_L^*$ and $\mathrm{n}_O\pi_L^*$ characters are more mixed in the FC position. Increasing this CO bond-length, the two states mix, so that the lowest adiabatic state deriving from their combination acquires a more clear $\mathrm{n}_O\pi_L^*$ character.

Inter-state couplings between states of different symmetry are triggered by non-total symmetric modes. Also in this case the modes that contribute most are the same for both functionals but, due to the different nature of the diabatic $\mathrm{n}\pi_L^*$ states, the specific contribution of each mode to the couplings of each of $\pi_H\pi_L^*$ and $\pi_1\pi_L^*$ with the two $\mathrm{n}\pi_L^*$ can exhibit significant differences.

For getting additional information on the origin of the main differences of the predictions of the time evolution of the electronic populations with PBE0 and CAM-B3LYP functionals in the next sections we report cuts of the LVC potentials along some relevant coordinates, i.e. those connecting the FC point to the diabatic minima of the first two $\pi\pi^*$ and nπ^* states.

S2.3 1D cuts of the LVC potential energy surfaces

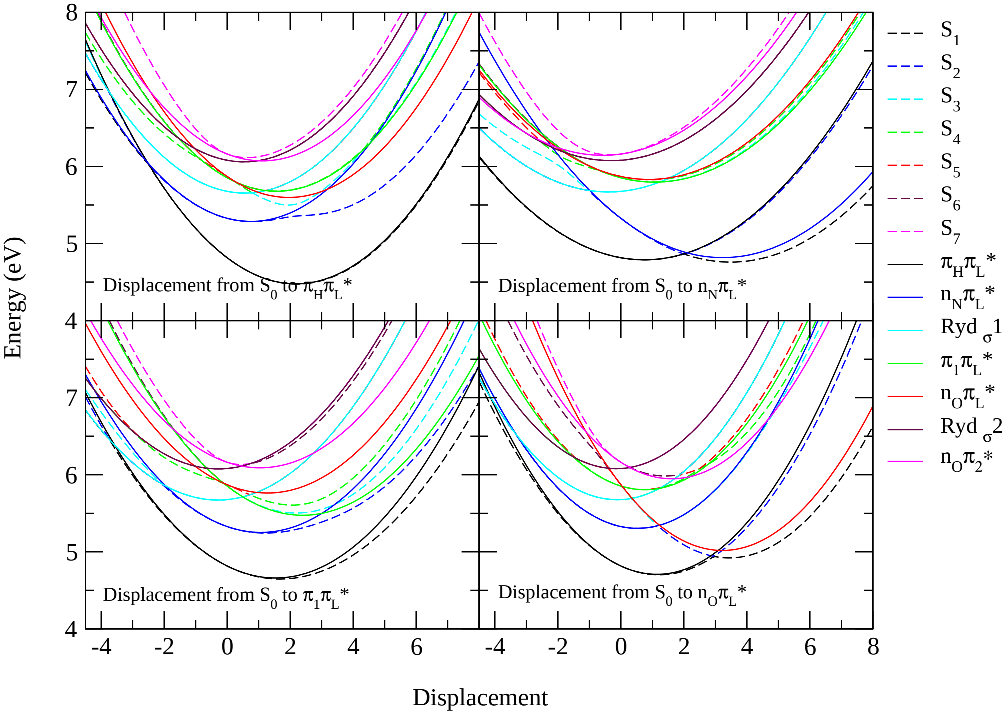

Figure S13: 1D energy profile of adiabatic (dash lines) and diabatic (solid line) potential energy surfaces (PES) along a coordinate connecting the FC point to the minima of the first bright state (top left), the first dark state (top right), the second bright state (bottom left), obtained by LVC Hamiltonians parameterized with CAM-B3LYP calculations.

Figures S13 and S14 report one dimensional (1D) cuts of the LVC diabatic and adiabatic PES along the coordinates connecting the ground state minimum (at position 0) with the diabatic minima of the first two lowest $\pi\pi^*$ and $n\pi^*$ states. It is interesting to highlight that even simple LVC models predict that the different states form an intricate network of crossing, with many local minima on the adiabatic states, giving a first explanation to the complex photoexcited dynamics observed in experiment. Strong couplings between $n\pi^*$ states introduce remarkable difference between the diabatic (solid) and adiabatic (dashed) PES. This is more clearly seen in PBE0 PES considering $\mathrm{n}_O\pi^*_L$+$\mathrm{n}_N\pi^*_L$ and $\mathrm{n}_O\pi^*_L$-$\mathrm{n}_N\pi^*_L$

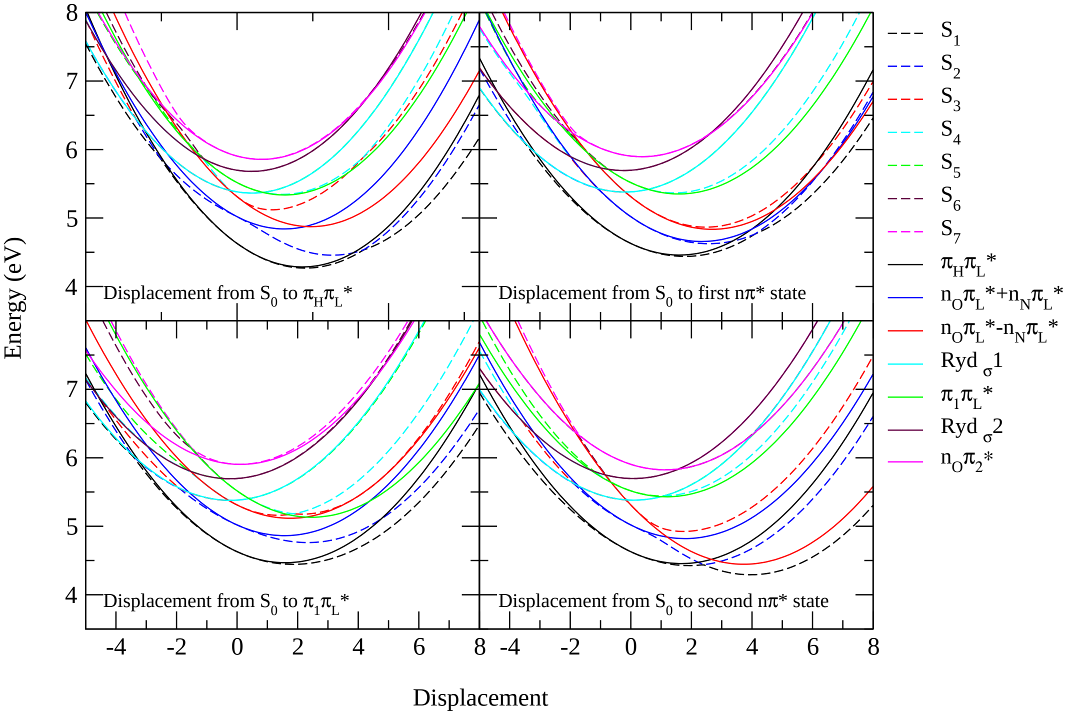

Figure S14: 1D energy profile of adiabatic (dash lines) and diabatic (solid line) potential energy surfaces (PES) along a coordinate connecting the FC point to the minima of the first bright state (top left), the first dark state (top right), the second bright state (bottom left), obtained by LVC Hamiltonians parameterized with PBE0 calculations.

diabatic states. Moving toward the minimum of $n_O\pi_L^*$-$n_N\pi_L^*$ this state becomes even more stable than $\pi_H\pi_L^*$ so that the lowest-energy adiabatic state S_1 acquires a nπ^* character. The same happens for CAM-B3LYP PES and also in this case S_1 exhibits a minimum with nπ^* character. However, at variance with PBE0 this local minimum is less stable than the minimum with the $\pi_H\pi_L^*$ character. For both functionals these energy profiles suggest that after an initial photoexcitation to the second bright state ($\pi_1\pi_L^*$) a rich pattern of crossings can lead quickly the excited population to the lower energy states.

S2.3.1 Comparison of TD-DFT and LVC adiabatic PES

In Figures S15 (CAM-B3LYP) and S16 (PBE0) we consider the same collective coordinates adopted in the previous two figures and we compare the 1D profiles of the three lowest adiabatic PES predicted by the LVC models with the corresponding TD-DFT energies. It can be seen that along all coordinates the LVC energy profiles are remarkably accurate with a partial exception for the coordinate (dominated by the C=O stretching) that leads from S0 minimum to the minimum of the second nπ^* state, which corresponds to a minimum with $\mathrm{n}_0\pi^*_L$ character. For values of this collective coordinate > ∼1.5 which is in the vicinity of the $\pi_H\pi^*_L$ minimum, the lowest adiabatic energy predicted by LVC increases more steeply than the TD-DFT one. As a consequence, the crossing with the second adiabatic PES (corresponding to a nπ^* state with main $\mathrm{n}_0\pi^*_L$ character) occurs at smaller values of the coordinate in the LVC case. After that crossing, the lowest-energy adiabatic state switch character from $\pi_H\pi^*_L$ to $\mathrm{n}_0\pi^*_L$.

S2.3.2 Quadratic correction to the LVC PES of $\pi_H\pi^*_L$ state along the C=O stretching

As discussed in the previous section, comparison of LVC and TD-DFT adiabatic PES indicate that, along the collective coordinate connecting the GS minimum with the nπ^* minimum with main $\mathrm{n}_0\pi^*_L$ character, dominated by the C=O stretching, TD-DFT lowest-energy PES (with $\pi_H\pi^*_L$ character) is flatter than the LVC model PES. We computed the the excited-state frequencies of the $\pi_H\pi^*_L$ adiabatic state (S1) in its own minimum at both PBE0 and CAM-B3LYP level of theory and we compared the S1 and GS normal modes analysing the Duschinsky matrix with the tools available in our distributed code *FCclasses*.[1] At CAM-B3LYP level the GS mode 42 is projected on several modes of the S1 excited-state (9 of them

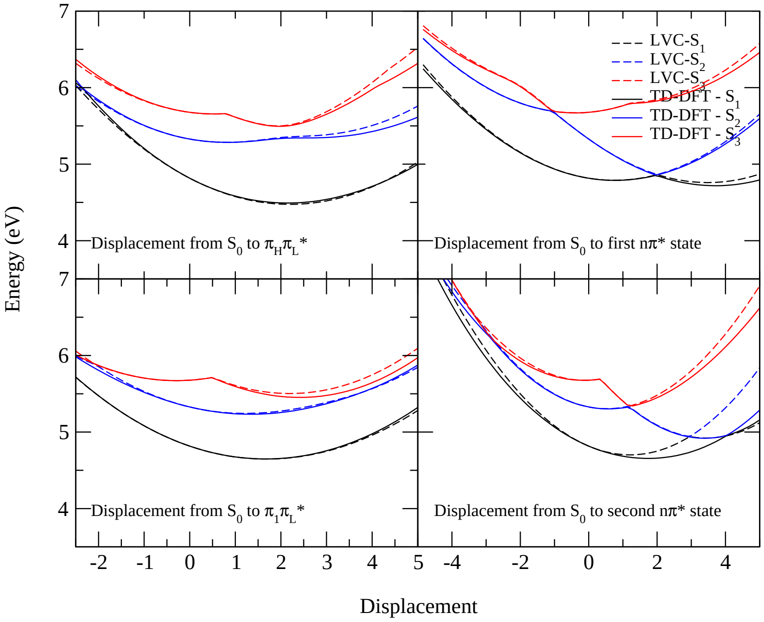

Figure S15: 1D energy profile of first three adiabatic PES along a coordinate connecting the FC point to the minima of the first bright state (top left), the first dark state (top right), the second bright state (bottom left) obtained by LVC Hamiltonians (dash line) and TD-DFT (solid-line) with CAM-B3LYP calculation.

are necessary to have a projection $>$ 90%). The largest projection (22%) is with mode 36 (1480 cm^{-1}) and the second largest (17%) with mode 29 (1260 cm^{-1}). At PBE0 level, the situation is similar: 8 S1 modes are necessary to have a projection of the GS mode 42 $>$ 90%, the largest contribution (29%) is given by S1 mode 28 (1230 cm^{-1}) and the second largest contribution (24%) by mode 27 (1180 cm^{-1}). This indicates that mode 42 is affected by relevant quadratic couplings (also those off-diagonal causing the Duschinsky mixing) and that its "effective" frequency in S1 is much smaller than in GS. This analysis strongly suggests that the discrepancy between the LVC and TD-DFT S1 PES observed in Figures S15 and S16 is due, at least partially, to a decrease of the frequency of mode 42 in S1 that is not accounted for by LVC model. Therefore we introduced in the LVC Hamiltonian a quadratic term -$\Delta\Omega q_{42}^2$ to reproduce as much as possible the TD-DFT profile along the collective coordinate connecting the GS and n$_0\pi_L^*$ minima. Figure S17 reports

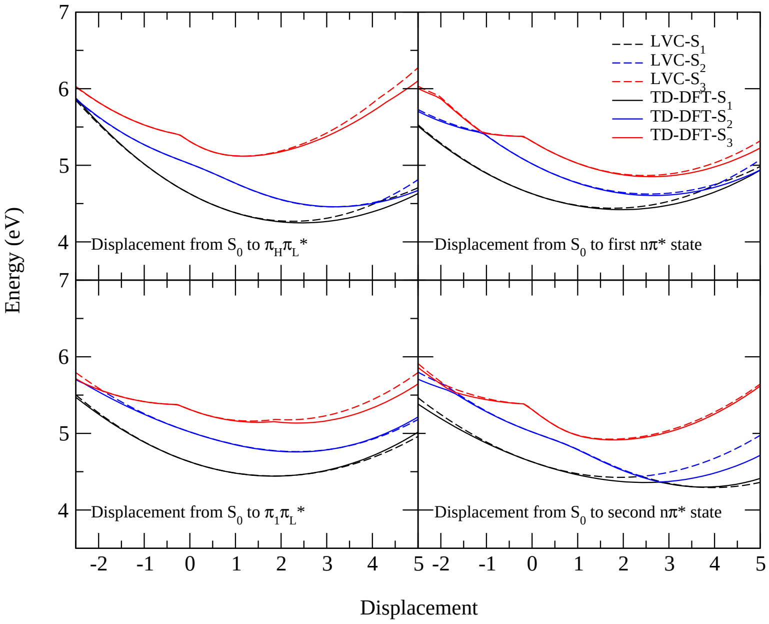

Figure S16: 1D energy profile of first three adiabatic PES along a coordinate connecting the FC point to the minima of the first bright state (top left), the first dark state (top right), the second bright state (bottom left) obtained by LVC Hamiltonians (dash line) and TD-DFT (solid-line) with PBE0 calculation.

the resulting ”LVC-Frequency-shift” PES showing that they now are very close to the TD-DFT ones. The estimated value of the frequency correction $\Delta\Omega$ is $\sim$ 1100 cm^{-1} for CAM-B3LYP and $\sim$ 700 cm^{-1} for PBE0. This correction is larger than expected from the analysis of the computed S1 frequencies, in particular for CAM-B3LYP, thus highlighting that concentrating all the correction on the frequency of mode 42 we make an approximation. Luckily this approximation is not a problem for CAM-B3LYP, at least for a dynamics initiated on $\pi_H\pi_L^*$, since the population remains on this state and the motion along the C=O mode is limited.

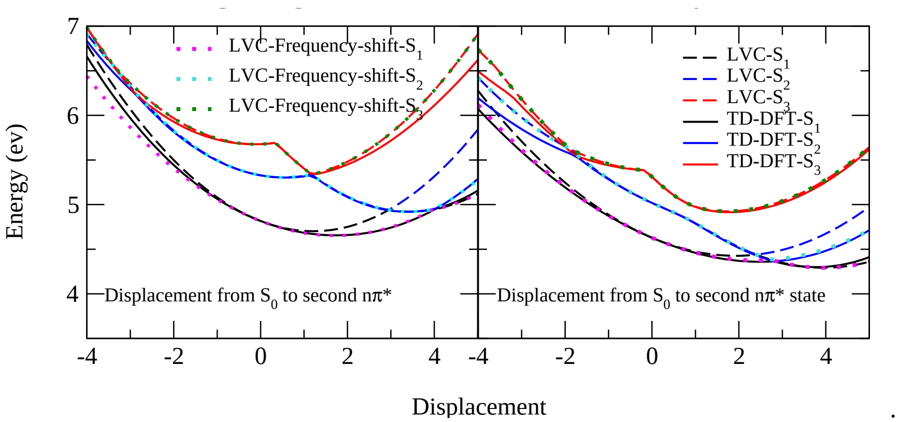

Figure S17: 1D energy profile of first three adiabatic PES along a coordinate connecting the FC point to the minima of the first bright state (top left), the first dark state (top right), the second bright state (bottom left) obtained by LVC Hamiltonians (dash line), TD-DFT (solid-line) and LVC Hamiltonian with frequency shift $\Delta\Omega$ of mode 42 with CAM-B3LYP ($\sim$ 1100 cm^{-1}) (left) and PBE0 ($\sim$ 700 cm^{-1}) (right) calculations.

S2.4 Discussion on LVC and TD-DFT excited-state minima

Tables S15 (CAM-B3LYP) and S21 (PBE0) report the energies of all diabatic states at the minima of all diabatic states computed within LVC model. These minima all belong to C$_s$ symmetry by construction. According to CAM-B3LYP, $\pi_H\pi_L^*$ is the lowest-energy diabatic state in its minimum. The same is true for $n_N\pi_L^*$ and for $n_O\pi_L^*$. However, it is worthy to notice that the latter state in its minimum is still very close ($<$ 0.05 eV) to the $\pi_H\pi_L^*$ state. The diabatic state $\pi_1\pi_L^*$ in its minimum is less stable than both $\pi_H\pi_L^*$ and $n_N\pi_L^*$.

According to PBE0, $\pi_H\pi_L^*$ is the lowest-energy diabatic state in its minimum. The same is true for $n_O\pi_L^*$-$n_N\pi_L^*$, although it is the third diabatic state in order of increasing energy at the FC position. At variance, $n_O\pi_L^*$+$n_N\pi_L^*$, i.e. the second diabatic state in the FC position, in its minimum is still less stable than $\pi_H\pi_L^*$. Finally $\pi_1\pi_L^*$ in its minimum is the third diabatic state, being less stable than $\pi_H\pi_L^*$ and $n_O\pi_L^*$+$n_N\pi_L^*$. It is worthy to notice that since LVC model also includes couplings along total-symmetric modes between states of the same symmetry, these diabatic minima may not coincide with adiabatic LVC minima. In practice even when a diabatic state is the most stable in its own minimum, a mixing with a state of the same symmetry can give rise to a more stable adiabatic state. Clearly, the latter would still be $\pi\pi^*$ or nπ^* but, at the same time, it would show some mixing of the diabatic characters.

This is actually what happens in Figures S13 (CAM-B3LYP) and S14 (PBE0) where the adiabatic PES do not coincide with the diabatic ones. In particular in Figure S13, in the vicinity of the $n_N\pi_L^*$ diabatic minimum, the S1 LVC energy is slightly lower than the diabatic one; the same happens in the vicinity of the $n_O\pi_L^*$ diabatic minimum. In both cases, according to the LVC model, both $n_N\pi_L^*$ and $n_0\pi_L^*$ minima correspond to minima on the S1 PES, but they are still close to the adiabatic state with $\pi_H\pi_L^*$ character (especially $n_0\pi_L^*$). At the position of the minimum with $\pi_H\pi_L^*$ character the diabatic and adiabatic energies practically coincide, because the second diabatic $\pi\pi^*$ state, $\pi_1\pi_L^*$ is too high in energy to effectively mix with $\pi_H\pi_L^*$.

This picture generally agrees well with what found with optimizations of the adiabatic states with TD-DFT. Considering CAM-B3LYP data, the minimum with $\pi_H\pi_L^*$ character is the lowest-energy minimum on S1 (Section S1.1.3) and the minimum with n$_N\pi_L^*$ is a local minimum on S1 (Section S1.1.4). Concerning the minimum with n$_O\pi_L^*$ character. According to TD-DFT it is a minimum on S2, 0.15 eV above S1 ($\pi_H\pi_L^*$), while according to LVC it is a minimum on S1. We showed that this is due to an overestimation of the frequency of mode 42 in the $\pi_H\pi_L^*$ diabatic state. Applying the quadratic correction the n$_O\pi_L^*$ minimum is correctly placed on the S2 adiabtic surface (see Figure S17).

Considering PBE0 data (Section S1.2.3), the minimum with $\pi_H\pi_L^*$ character is the lowest-energy minimum on S1 and the minimum with n$_N\pi_L^*$ is a local minimum on S1, in agreement with what seen in Figure S14. Concerning n$_O\pi_L^*$, as reported above, we were not able to locate its minimum by TD-DFT. Nonetheless we documented that there is a region of the coordinate space, along the coordinate connecting the GS and the $n_O\pi_L^*$-$n_N\pi_L^*$ minima where S1 has a clear n$_O\pi_L^*$ character (starting from there we found a point where S1 has n$_O\pi_L^*$ and an energy lower than it has in the $\pi_H\pi_L^*$). This picture is similar to what found with LVC model where, however, the crossing between $\pi_H\pi_L^*$ and the nπ^* states occurs for smaller displacements from the GS minimum (Figure S16). This inaccuracy is corrected accounting for a decrease of the frequency of mode 42 in the $\pi_H\pi_L^*$ state (Figure S17).

S3 Additional results for the Dynamics

S3.1 Convergence test of the ML-MCTDH calculations

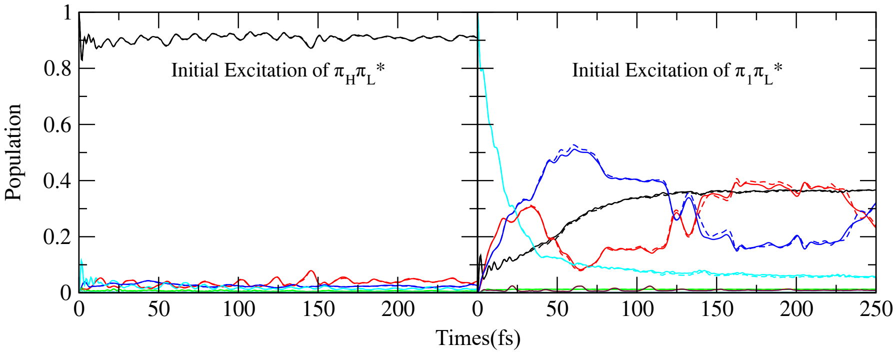

Figure S18: Convergence test for ML-MCTDH propagations with respect to the dimensions of the primitive basis set and the number of single particles (SPs). We considered the nonadiabatic dynamics of electronic populations of cytosine in gas phase predicted with LVC Hamiltonians parameterized the at the $\pi_H\pi_L^*$ minimum with CAM-B3LYP calculations.The time evolution adopted with the settings used in most of the calculations (”standard”, solid line) is compared with what obtained decreasing both the primitive basis set and the number of SPs (dashed line). A graphical representation of the multilayer (ML) tree is reported in Figure S20 for the small test case and in Figure S19 for the standard settings.

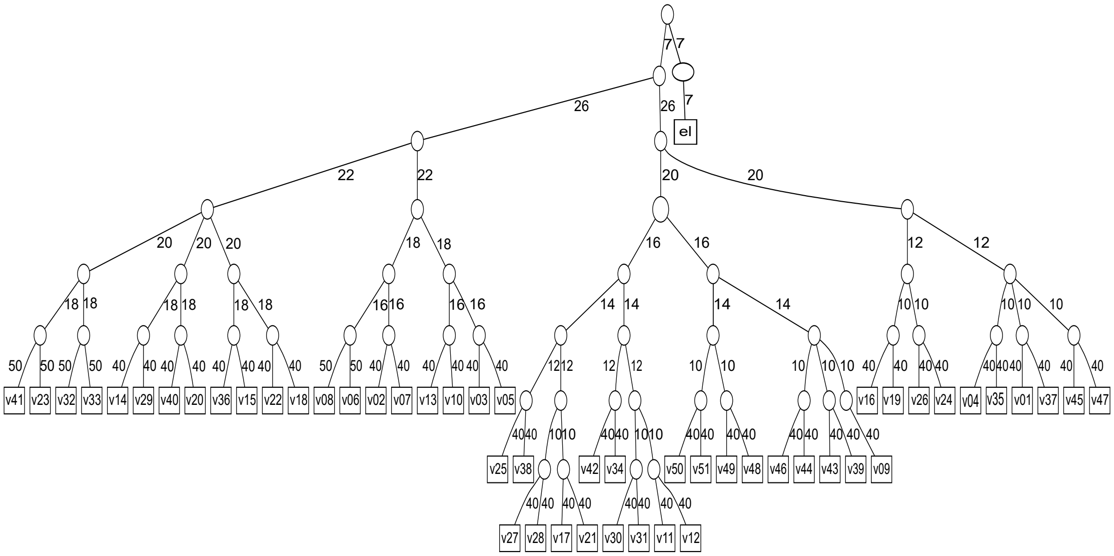

Figure S19: Graphical representation of a typical ML-MCTDH tree adopted in the computations.

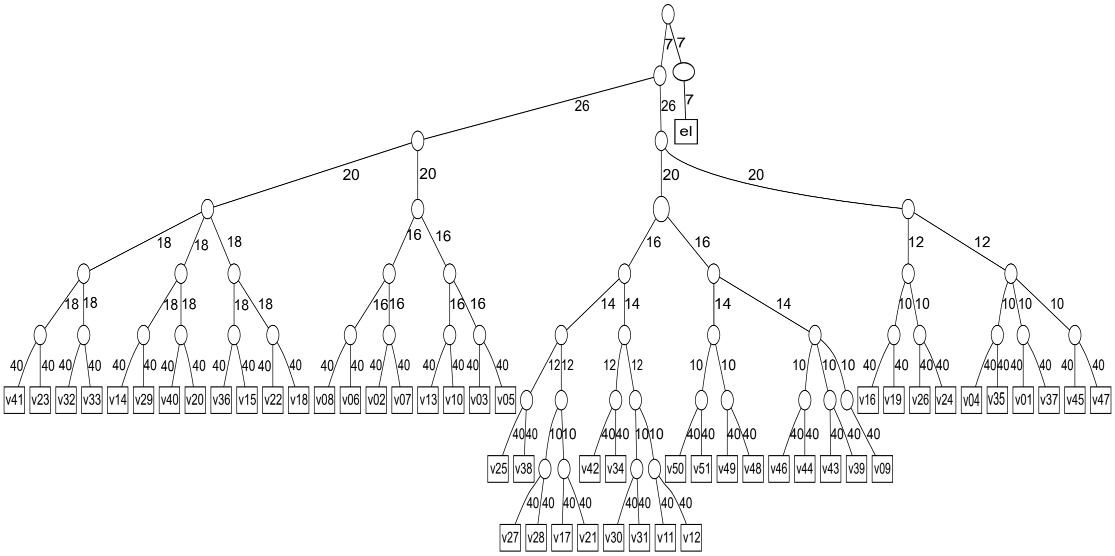

Figure S20: Graphical representation of the ML-MCTDH tree with smaller basis set and number of SPs adopted to check the convergence of the calculations made with standard settings (see Figure S19).

S3.2 Effect of mode 1 on the time evolution of electronic populations

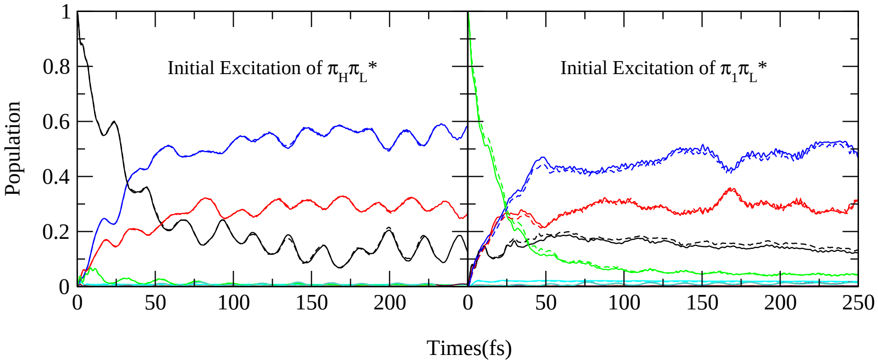

Figure S21: The time-evolution of the electronic populations reported in the main text for 1,5diMe-Cyt in gas-phase with a LVC parameterized in the FC position (solid lines) is compared with the results (dashed lines) when mode 1 is neglected for PBE0 calculation. Initial photoexcitation to $\pi_H\pi_L^*$ (left) or $\pi_1\pi_L^*$ (right).

S3.3 Dynamics with LVC Hamiltonians parametrized in the FC point

S3.3.1 Effect of Rydberg states on the time evolution of electronic populations

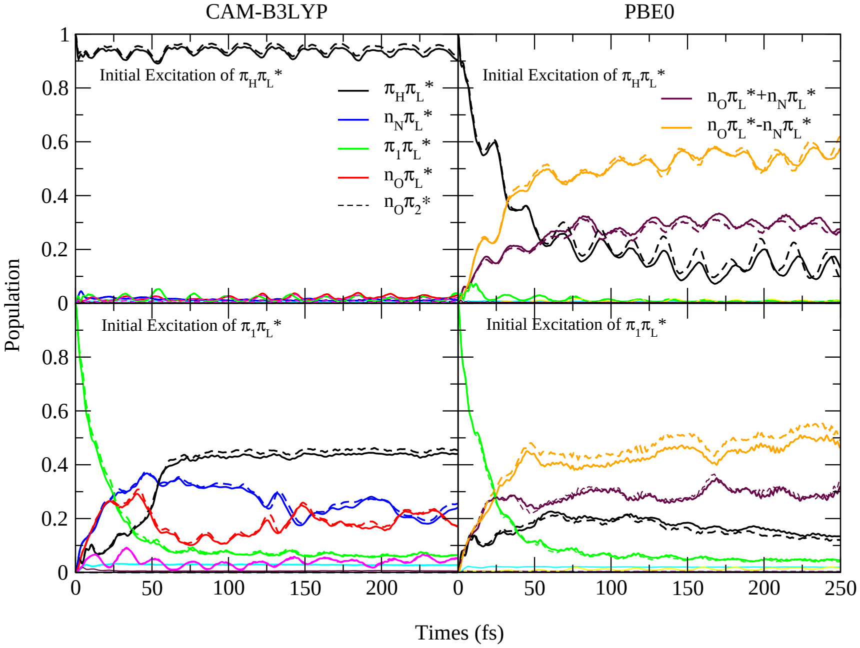

Figure S22: The time-evolution of the electronic populations reported in the main text for 1,5diMe-Cyt in gas-phase with a LVC parameterized in the FC position (solid lines) is compared with the results (dashed lines) when Rydberg states are neglected for CAM-B3LYP (left) and PBE0 (right) calculations.

S3.3.2 Dynamics with CAM-B3LYP Hamiltonians and PBE0 excitation energies and viceversa.

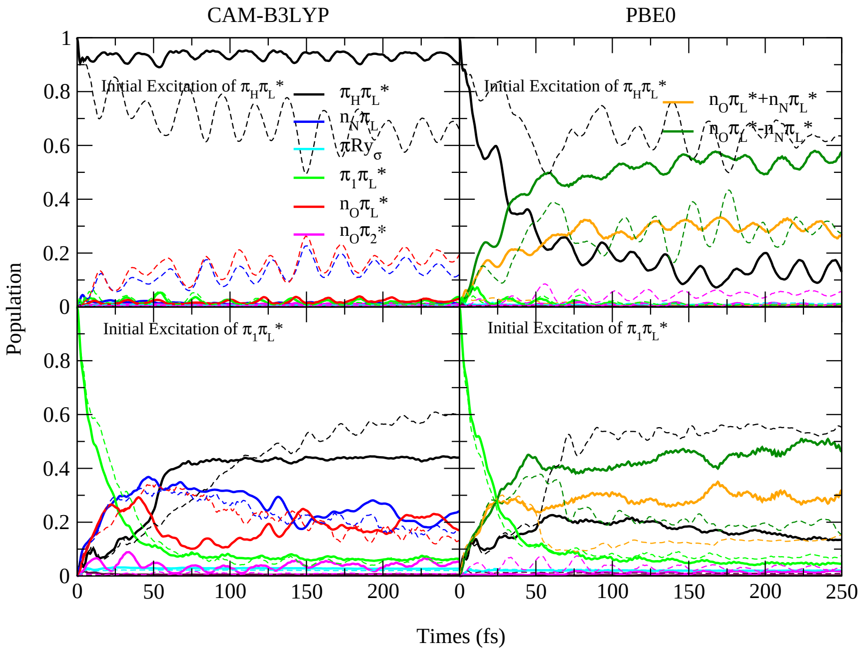

Figure S23: The time-evolution of the electronic populations reported in the main text for 1,5diMe-Cyt in gas-phase with a LVC parameterized in the FC position (solid lines) is compared with the results of LVC Hamiltonian of PBE0 with excitation energy of the CAM-B3LYP (dashed line in the left panels) and the LVC Hamiltonian of CAM-B3LYP with excitation energy of the PBE0 (dashed line in the right panel).

As discussed in Section S2.2 there are many analogies between the LVC parameters obtained with CAM-B3LYP and PBE0 but also remarkable differences, both in the vertical excitation energies and in inter- and intra-state couplings that involve nπ^* states, due to the fact that their nature is significantly different according to the two functionals. As a matter of fact, the two LVC models predict very different dynamics starting from both $\pi_H\pi_L^*$ and $\pi_1\pi_L^*$. In order to investigate the effect of the different stabilities in the ground state geometry, in Figure S23 we compare the results obtained with CAM-B3LYP (left panels) and PBE0 (right panels) and already reported in Figure 1 of the main text with those of modified Hamiltonians obtained replacing CAM-B3LYP vertical energies in the PBE0

Hamiltonian (left) and, conversely, PBE0 vertical energies in the CAM-B3LYP Hamiltonian (right). For dynamics starting from $\pi_1\pi_L^*$, results are rather clear. Replacing CAM-B3LYP energies in the PBE0 Hamiltonian decreases remarkably the population loss of $\pi_H\pi_L^*$, giving predictions intermediate between CAM-B3LYP and PBE0 original Hamiltonians. The same is found replacing PBE0 energies in the CAM-B3LYP Hamiltonian. This clearly indicates that differences in the vertical transition energies are a key factor in determining the different CAM-B3LYP and PBE0 dynamics, but also shows at the same time that, other factors, i.e. the different inter- and intra-site couplings predicted by the two functionals play a comparable role. The situation is more complex for dynamics starting on $\pi_1\pi_L^*$ since, although the decay of $\pi_1\pi_L^*$ of these two modified Hamiltonians is similar to those already predicted by the two original Hamiltonians, the population transfer to the two nπ_L^* states and to the lowest $\pi_H\pi_L^*$ state is more difficult to rationalize. This finding is in line with the fact that a dynamics with larger available kinetic energy and involving more states is more complex. These tests in any case show that differences in the vertical transition energies play a very important role but they are not able by themselves to completely explain the differences between the predictions of CAM-B3LYP and PBE0 LVC Hamiltonians.

S3.3.3 Dynamics from the lowest bright state $\pi_H\pi_L^*$

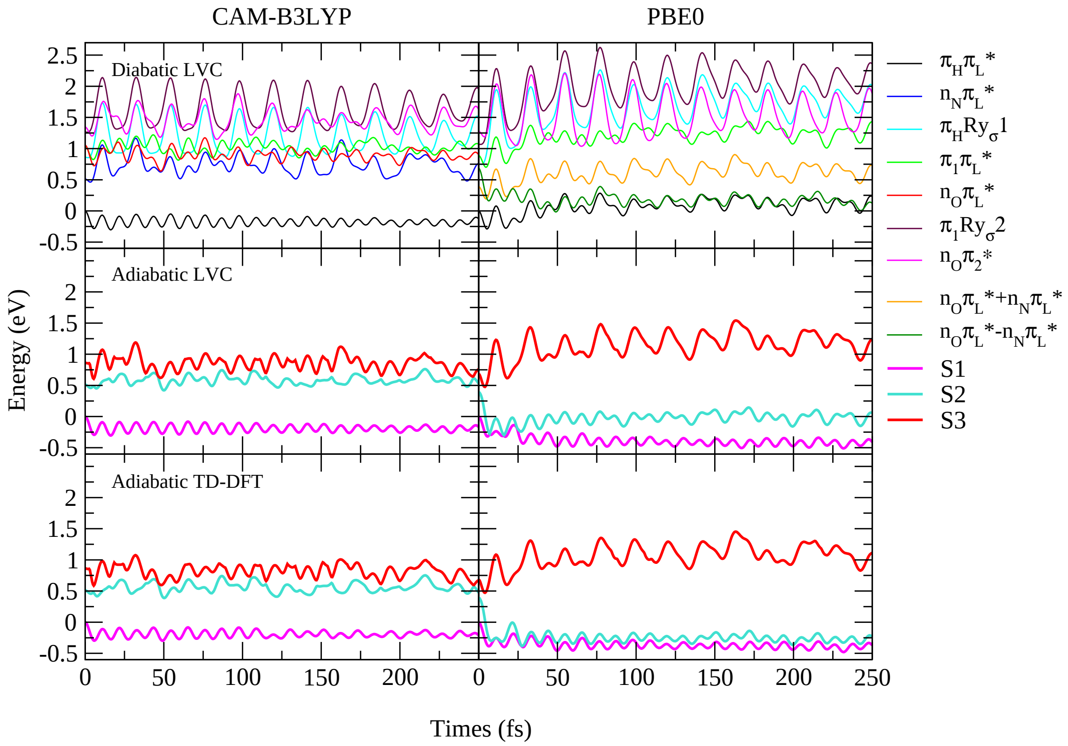

Figure S24: Diabatic (top) and adiabatic potential energies (middle, only for the three lowest states) in the average position of the wavepacket (C_s symmetry) obtained by LVC Hamiltonians parameterized with CAM-B3LYP (left) or PBE0 (right) calculations. The energy zero corresponds to the FC energy of the $\pi_H\pi_L^*$ state, i.e. respectively 4.81 eV for CAM-B3LYP and 4.62 eV for PBE0.For comparison we also report (bottom) the three lowest adiabatic energies recomputed by TD-DFT at molecular structures corresponding to the average position of the wavepacket.

Diabatic potentials at the average position of the wavepacket (WP), reported as a function of time in Figure S24 for an initial photoexcitation to $\pi_H\pi_L^*$, give a clear understanding of the difference of the dynamics with Hamiltonians parameterized with CAM-B3LYP and PBE0. According to CAM-B3LYP, $\pi_H\pi_L^*$ remains at all times well separated in energy from the other states, making difficult a population transfer. At variance, according to PBE0, $\pi_H\pi_L^*$ becomes practically degenerate with $n_O\pi_L^* - n_N\pi_L^*$ for t> 35 fs. A similar behavior is seen on the adiabatic PES recomputed with TD-DFT at molecular structures corresponding to the average position of the WP and reported in the bottom panels of the same Figure. At CAM-B3LYP level S1 remains quite separated from S2 and S3 that are almost degenerate, and Figure S25 indicates that while S1 has always $\pi_H\pi^*_L$ character, S2 and S3 switch between $n_O\pi^*_L$ and $n_N\pi^*_L$ characters. On the contrary, according to PBE0, S1 and S2 are practically degenerate along all the trajectory while S3 is significantly less stable. Figure S26 then shows that, except at the very beginning of the dynamics, S1, S2 and S3 have respectively $n_O\pi^*_L$, $\pi_H\pi^*_L$ and $n_N\pi^*_L$ characters. This helps to clarify that, although the diabatic nπ^*_L states adopted in the dynamics are mixed, from the adiabatic point of view the population leaving $\pi_H\pi^*_L$ clearly flows predominantly in a state with n$_O\pi^*_L$ character.

Finally the central panels of Figure S24 report the adiabatic energies predicted by the LVC Hamiltonian at the same geometries. At CAM-B3LYP level they are extremely similar to the TD-DFT ones, strongly supporting the reliability of the LVC approximation. As far as PBE0 results are concerned, comparing diabatic and adiabatic LVC PES we can notice that for times t$>$ 40 fs S2 adiabatic energy is quite similar to $\pi_H\pi^*_L$, and that the two diabatic $n\pi^*_L$ states ($n_O\pi^*_L$+$n_N\pi^*_L$ and $n_O\pi^*_L$-$n_N\pi^*_L$) split remarkably to form S1 and S3. This is confirmed by the assignments of the adiabatic TD-DFT states (recall that S1 is $n_O\pi^*_L$ and S3 is $n_N\pi^*_L$). At variance with TD-DFT results however, where S1 and S2 are almost degenerate, S2 LVC energy is significantly less stable than S1, suggesting that the population transfer from $\pi_H\pi^*_L$ to $n\pi^*_L$ states can be overestimated.

State) t(fs)	S_1	S_2	S_3
0	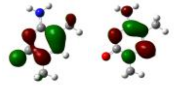 H→L($\pi\pi^*$)	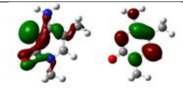 H-3→L($n_{mixed}\pi^*$) 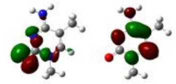 H-2→L($n_{mixed}\pi^*$)	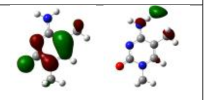 H→L+1(πRy_{σ})
50	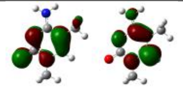 H→L($\pi\pi^*$)	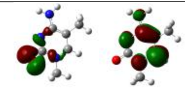 H-1→L($n_O\pi^*$)	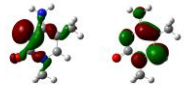 H-3→L($n_{mixed}\pi^*$)
100	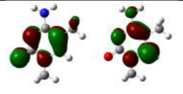 H→L($\pi\pi^*$)	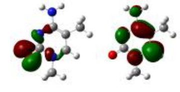 H-1→L($n_O\pi^*$)	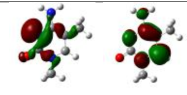 H-3→L($n_{mixed}\pi^*$)
150	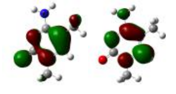 H→L($\pi\pi^*$)	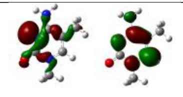 H-3→L($n_{mixed}\pi^*$)	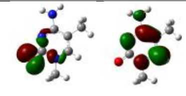 H-2→L($n_O\pi^*$)
200	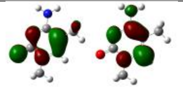 H→L($\pi\pi^*$)	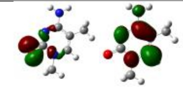 H-1→L($n_O\pi^*$)	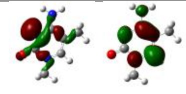 H-3→L($n_{mixed}\pi^*$) 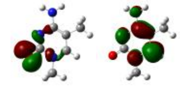 H-1→L($n_O\pi^*$)
250	 H→L($\pi\pi^*$)	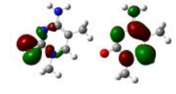 H-1→L($n_O\pi^*$)	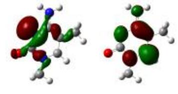 H-3→L($n_{mixed}\pi^*$)

Figure S25: Electronic character of the lowest three TD-DFT excited states computed at CAM-B3LYP/6-31+G(d,p) level of theory for structures corresponding to the average wavepacket position every 50 fs for a dynamics starting on the lowest $\pi_H\pi_L^*$ state.

State) t(fs)	S_1	S_2	S_3
0	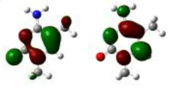 H→L($\pi\pi^*$)	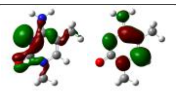 H-3→L($n_{mixed}\pi^*$) 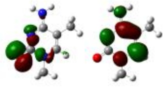 H-2→L($n_O\pi^*$)	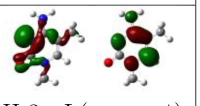 H-3→L($n_{mixed}\pi^*$) 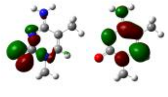 H-2→L($n_O\pi^*$)
50	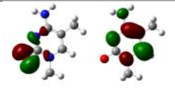 H-1→L($n_O\pi^*$)	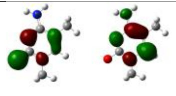 H→L($\pi\pi^*$)	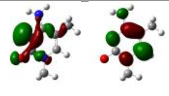 H-3→L($n_{mixed}\pi^*$)
100	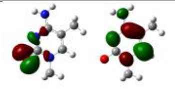 H-1→L($n_O\pi^*$)	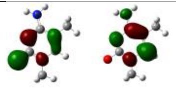 H→L($\pi\pi^*$)	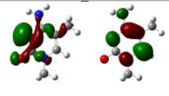 H-3→L($n_{mixed}\pi^*$)
150	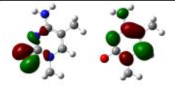 H-1→L($n_O\pi^*$)	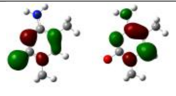 H→L($\pi\pi^*$)	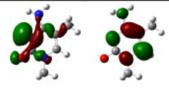 H-3→L($n_{mixed}\pi^*$)
200	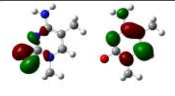 H-1→L($n_O\pi^*$)	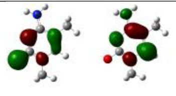 H→L($\pi\pi^*$)	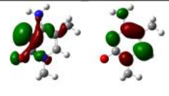 H-3→L($n_{mixed}\pi^*$)
250	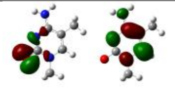 H-1→L($n_O\pi^*$)	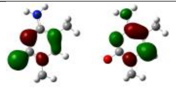 H→L($\pi\pi^*$)	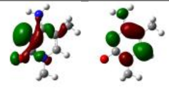 H-3→L($n_{mixed}\pi^*$)

Figure S26: Electronic character of the lowest three TD-DFT excited states computed at PBE0/6-31+G(d,p) level of theory for structures corresponding to the average wavepacket position every 50 fs for a dynamics starting on the lowest $\pi_H\pi_L^*$ state.

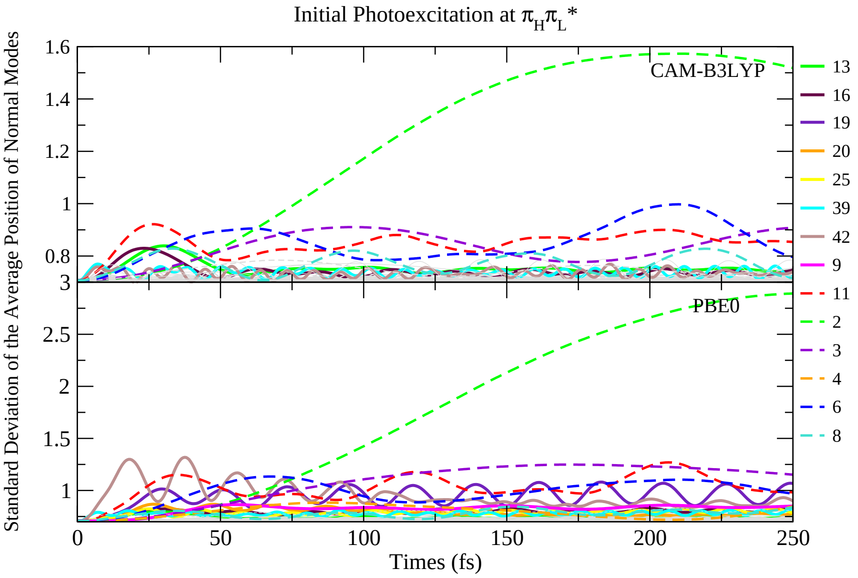

Figure S27: Standard deviation of the average position of $A^{'}$ (solid line) and $A^{''}$ normal modes obtained by LVC Hamiltonians parameterized with CAM-B3LYP (top) or PBE0 (bottom) calculations for initial photoexcitation of $\pi_H\pi_L^*$.

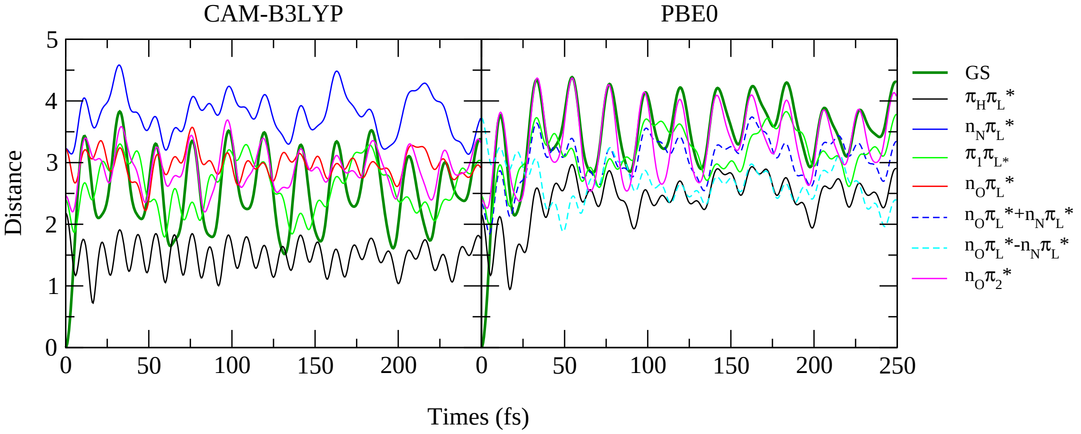

Figure S28: Distance (in dimensionless coordinates) of the trajectory of the average position of the wavepacket from different diabatic minima obtained by LVC Hamiltonians parameterized with CAM-B3LYP (left) or PBE0 (right) calculations at the FC positiom.

S3.3.4 Dynamics from the second bright state $\pi_1\pi_L^*$

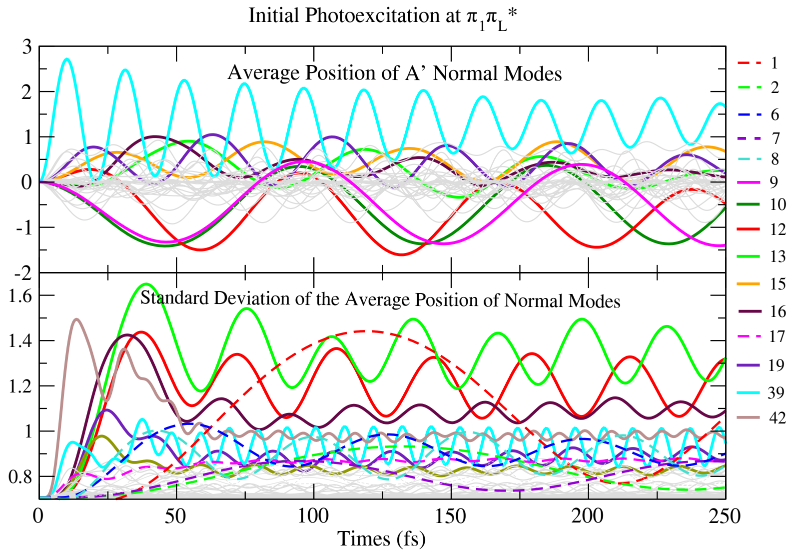

Figure S29: Expectation values of average positions of $A^{'}$ modes (TOP) and standard deviation of the average position of $A^{'}$ (solid line) and $A^{''}$ normal modes obtained by LVC Hamiltonians parameterized with CAM-B3LYP for initial photoexcitation of $\pi_1\pi_L^*$.

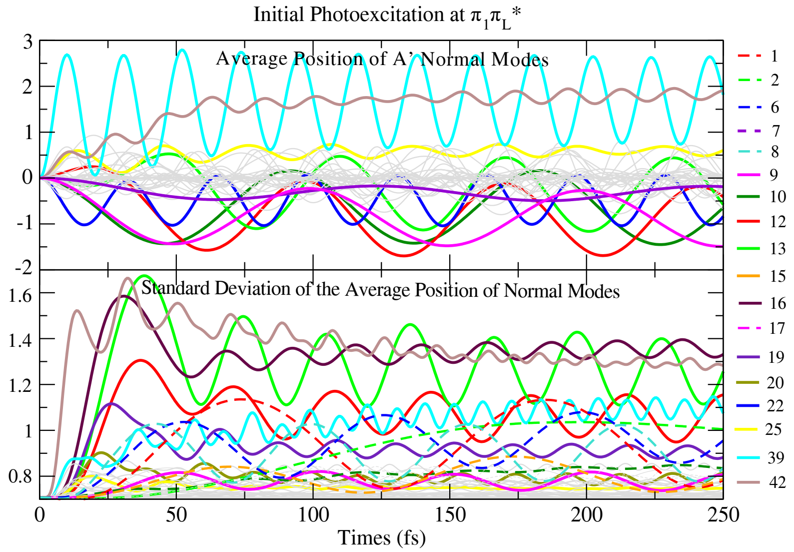

Figure S30: Expectation values of average positions of $A^{'}$ modes (TOP) and standard deviation of the average position of $A^{'}$ (solid line) and $A^{''}$ normal modes obtained by LVC Hamiltonians parameterized with PBE0 for initial photoexcitation of $\pi_1\pi_L^*$.

The richer dynamics after an excitation to $\pi_1\pi_L^*$ is also seen from the motion of the bond stretchings reported in Figure S31, which is even less regular and more

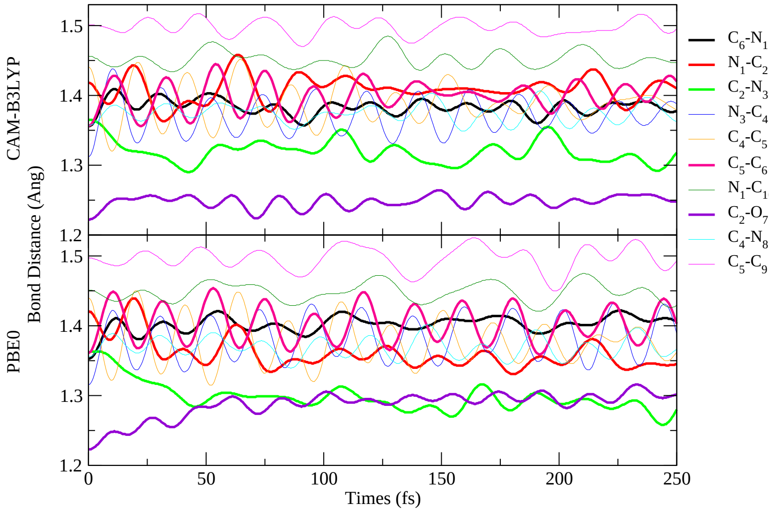

Figure S31: Bond Distance in the average position of the wavepacket (C_s symmetry) obtained by LVC Hamiltonians parameterized with CAM-B3LYP (top) or PBE0 (bottom) calculations for initial photoexcitation of $\pi_1\pi^*_L$.

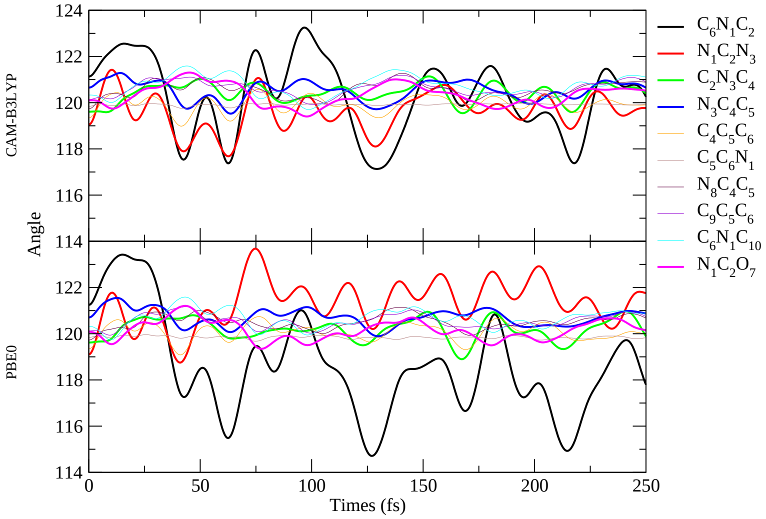

Figure S32: Bending angles in the average position of the wavepacket (C_s symmetry) obtained by LVC Hamiltonians parameterized with CAM-B3LYP (top) or PBE0 (bottom) calculations for initial photoexcitation of $\pi_1\pi^*_L$.

damped, despite the fact that, in principle, the vibrational energy is larger than for an excitation to $\pi_H\pi^*_L$. The dynamics of the bond angles for an initial excitation on $\pi_H\pi^*_L$ or on $\pi_1\pi^*_L$ is also different, although the minimum and maximum values reached in the oscillations are similar.

Differences are also seen in PBE0 despite the time evolution of the electronic populations is similar. Even for an excitation to $\pi_1\pi_L^*$, in fact, mode 42 shows a large motion which practically stops at t >70 fs, around values quite different from the initial ones (Figure S30). The same kind of behaviour is observed for other bond lengths. In fact in the first $\sim$ 50 fs timescale C_2-O_7 increases steeply while N_1-C_2 and C_2-N_3 decrease remarkably. Moreover, also the dynamics of bending angles is rather similar (compare Figures S32 with the corresponding Figure in the manuscript). Notwithstanding this, the much larger values of σ along several A$'$ modes clearly indicate differences in the WP dynamics. In fact, the WP feels the effect of different electronic states and spread much more in the coordinate space.

S3.3.5 Additional data for the comparison of the dynamics in 1Me-Cyt and 1,5diMe-Cyt

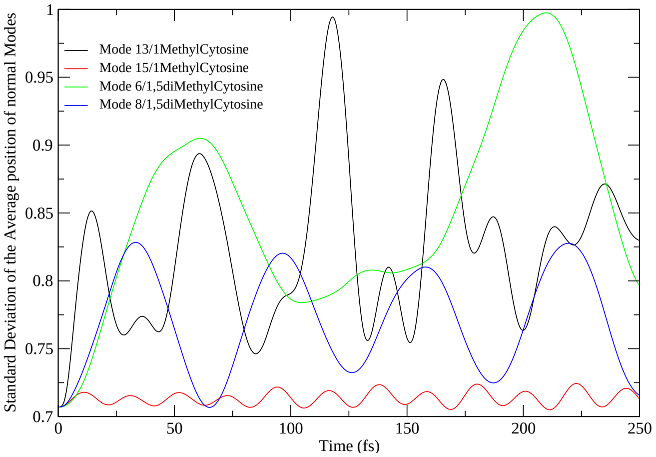

Figure S33: Standard deviation of the average position of modes 6 and 8 of 1,5diMe-Cyt and 13 and 15 of 1Me-Cyt obtained by LVC Hamiltonians parameterized with CAM-B3LYP calculations for initial photoexcitation of $\pi_H\pi_L^*$.

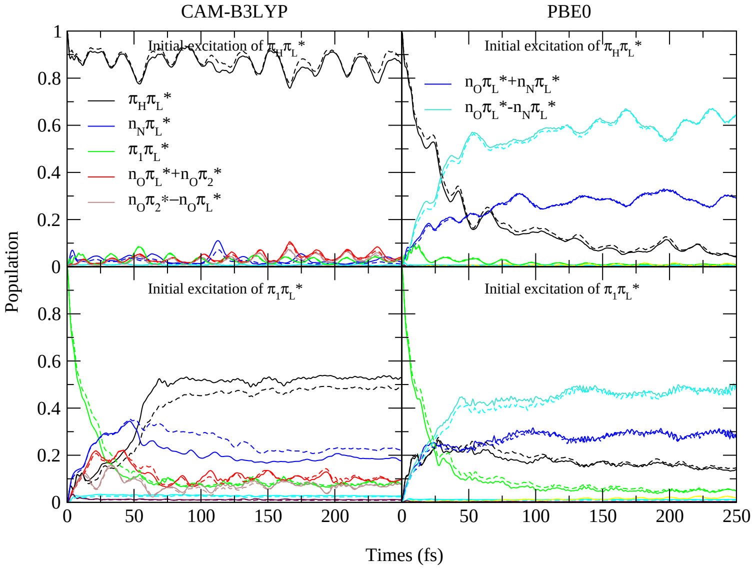

Figure S34: The time-evolution of the electronic populations reported in the main text for 1Me-Cyt in gas-phase with a LVC parameterized in the FC position (solid lines) is compared with the results (dashed lines) when mode 6 and 8 are neglected for CAM-B3LYP (left) and PBE0 (right) calculation. Initial photoexcitation to $\pi_H\pi_L^*$ (top) or $\pi_1\pi_L^*$ (bottom).

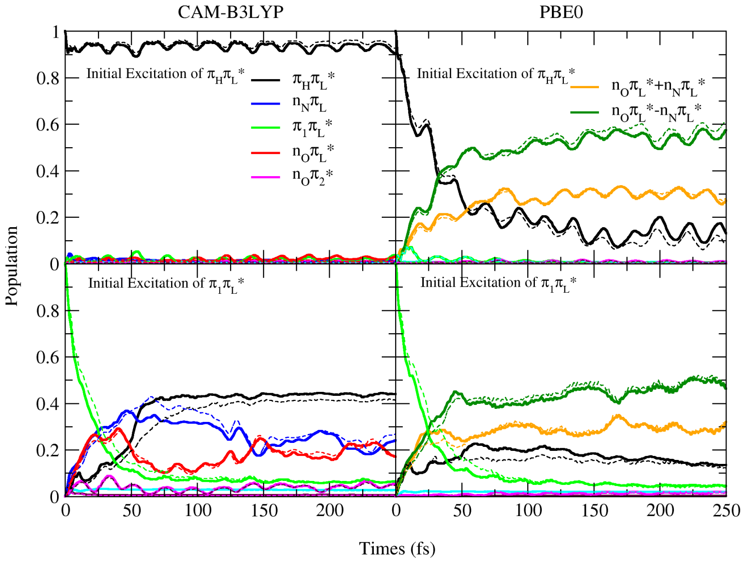

Figure S35: The time-evolution of the electronic populations reported in the main text for 1,5diMe-Cyt in gas-phase with a LVC parameterized in the FC position (solid lines) is compared with the results (dashed lines) when mode 6 and 8 are neglected for CAM-B3LYP (left) and PBE0 (right) calculation. Initial photoexcitation to $\pi_H\pi_L^*$ (top) or $\pi_1\pi_L^*$ (bottom).

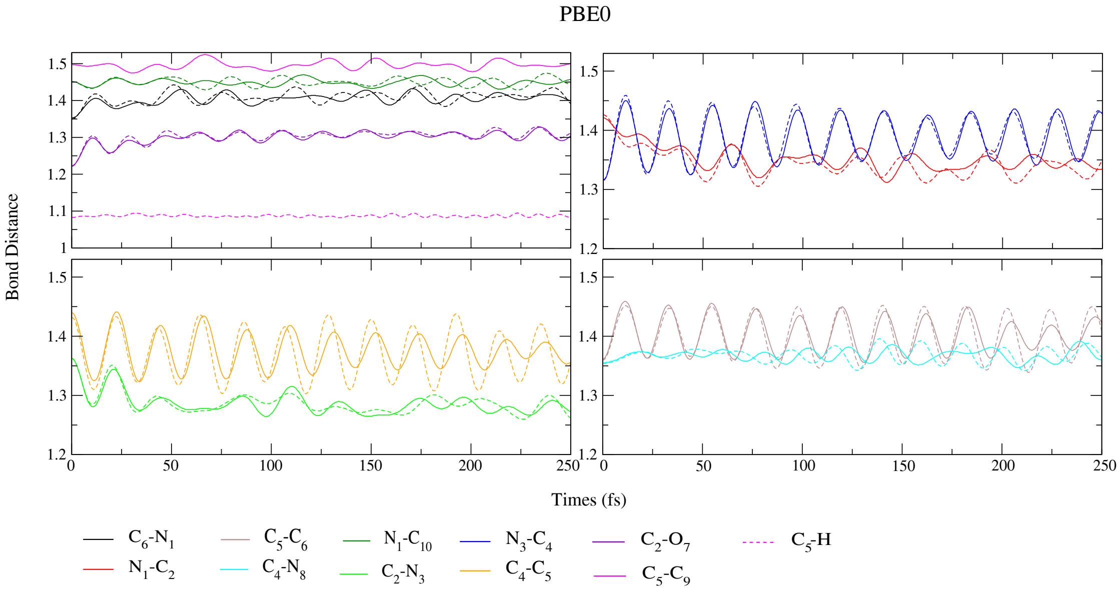

Figure S36: Comparison of bond distances of 1,5diMe-Cyt (solid lines) and 1Me-Cyt (dash lines) in the average position of the wavepacket (C_s symmetry) obtained by LVC Hamiltonians parameterized with PBE0 for initial photoexcitation of $\pi_H\pi_L^*$.

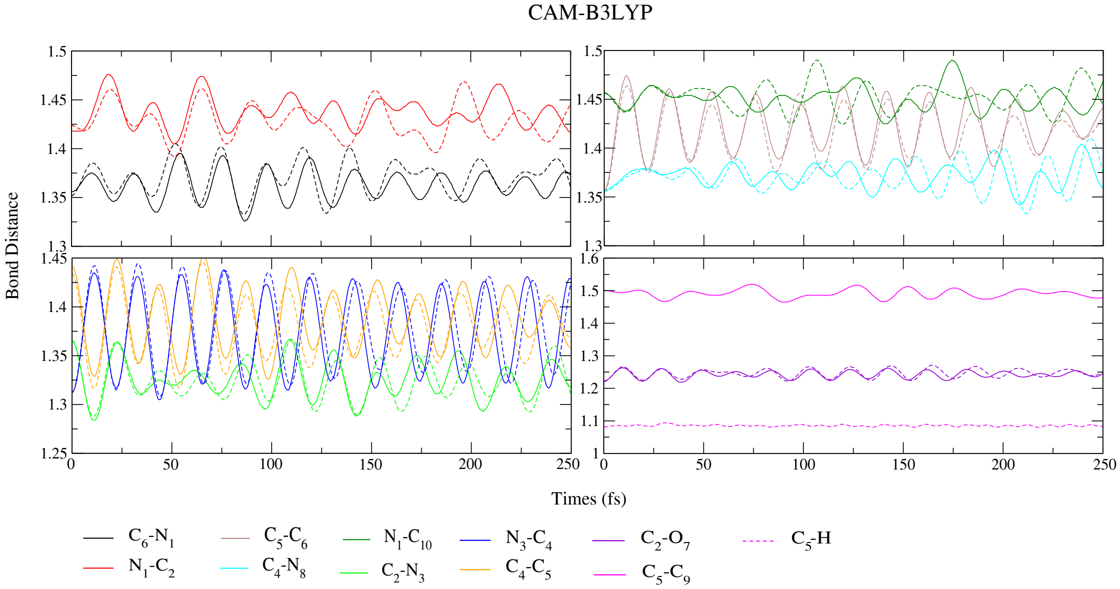

Figure S37: Comparison of bond distances of 1,5diMe-Cyt (solid lines) and 1Me-Cyt (dash lines) in the average position of the wavepacket (C_s symmetry) obtained by LVC Hamiltonians parameterized with CAM-B3LYP for initial photoexcitation of $\pi_H\pi_L^*$.

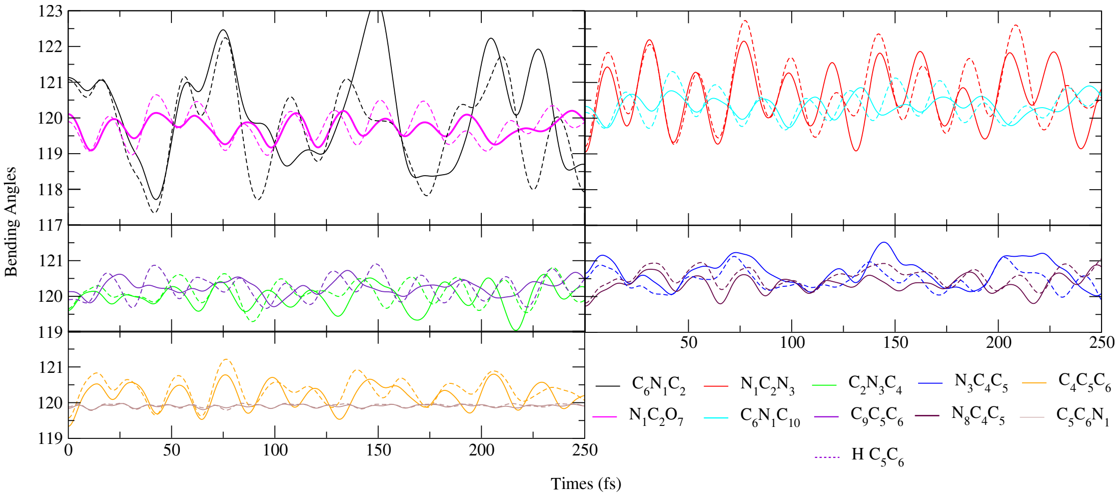

Figure S38: Comparison of the time evolution of bending angles of of 1,5diMe-Cyt (solid lines) and 1Me-Cyt (dash lines) in the average position of the wavepacket (C_s symmetry) obtained by LVC Hamiltonians parameterized with CAM-B3LYP, for initial photoexcitation of $\pi_H\pi_L^*$.

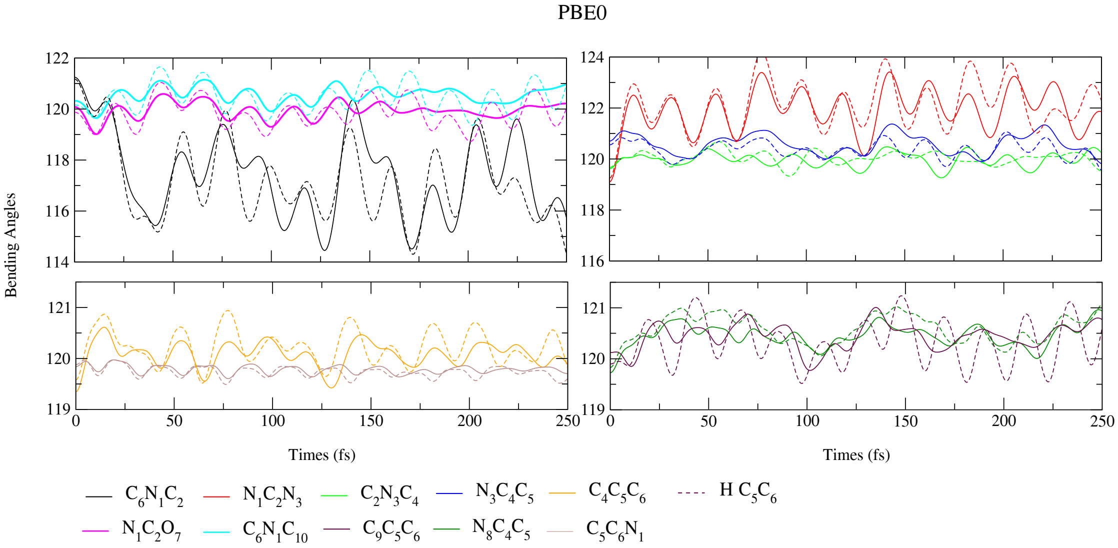

Figure S39: Comparison of the time evolution of bending angles of of 1,5diMe-Cyt (solid lines) and 1Me-Cyt (dash lines) in the average position of the wavepacket (C_s symmetry) obtained by LVC Hamiltonians parameterized with PBE0, for initial photoexcitation of $\pi_H\pi_L^*$.

S3.3.6 Dynamics with the LVC Hamiltonian parametrized for 1Me-Cyt and the excitation energies of 1,5diMe-Cyt

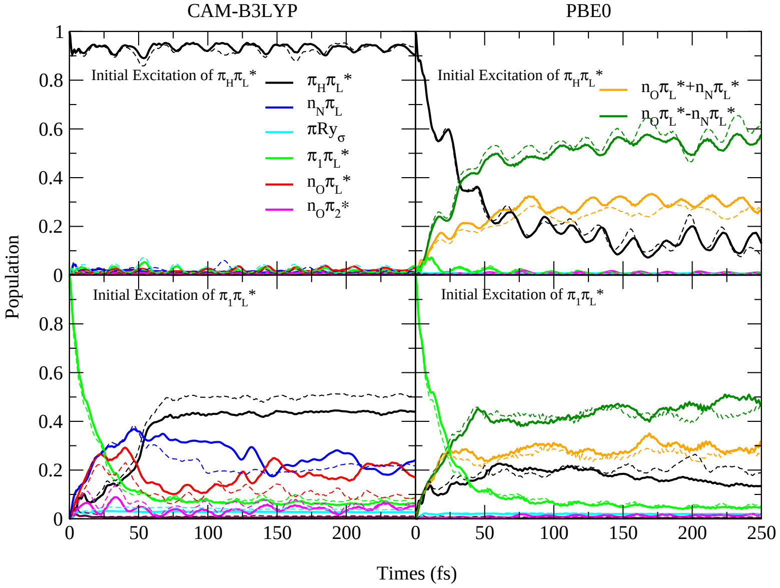

Figure S40: The time-evolution of the electronic populations reported in the main text for 1,5diMe-Cyt in gas-phase with a LVC parameterized in the FC position (solid lines) is compared with the results of the LVC Hamiltonian of 1Me-Cyt with excitation energy of 1,5diMe-Cyt with CAM-B3LYP (left) and PBE0 (right) calculations.

Figure S40 compares the time evolution of the electronic populations predicted for 1,5diMe-Cyt and for the LVC Hamiltonian parametrized for 1Me-Cyt modified replacing the vertical excitation energies with those of 1,5diMe-Cyt. Results should be compared also with those obtained with the original LVC Hamiltonian for 1Me-Cyt in Figure 1 in the main text. The very similar behaviour of solid and dashed lines in the top left panel proves that, for a dynamics started on $\pi_H\pi_L^*$, most of the differences observed at CAM-B3LYP level of theory between 1Me-Cyt and 1,5diMe-Cyt are due to the relative stability of the electronic states in the FC position and, in particular, to the stabilization of $\pi_H\pi_L^*$ in 1,5diMe-Cyt. At variance, comparison of the left-bottom panel with the one in Figure 1 shows that, at CAM-B3LYP level, replacing the vertical energies of 1Me-Cyt with those of

1,5diMe-Cyt, does not significantly change the dynamics of 1Me-Cyt, indicating that the (in any case) modest differences between 1Me-Cyt and 1,5diMe-Cyt, are induced by differences in the intra- or inter-state couplings. They are likely connected to the different extent of mixing of $n_O\pi_L^*$ and $n_O\pi_2^*$ characters in the second and third $n\pi^*$ states discussed in the main text. Figure 1 in the main text shows that PBE0 predicts even smaller differences between 1Me-Cyt and 1,5diMe-Cyt. In line with these results also the right panels of Figure S40 show slight differences.

S3.4 Dynamics with LVC Hamiltonians parameterized at the excited-state minima with CAM-B3LYP.

Table S22: Energies (E^a) of the adiabatic states of 1,5 dimethyl-cytosine in the minima of the first $\pi\pi^*$ and first two $\mathrm{n}\pi^*$ states and their electronic characters. E^d_{FC} are the energies, extrapolated at the FC point, of the diabatic states defined by LVC Hamiltonians parametrized at these minima. Energies in eV with respect to the ground state in its minimum. CAM-B3LYP/6-31+G(d,p) calculations in gas phase.

CAM-B3LYP								
First $\pi\pi^*$			First $\mathrm{n}\pi^*$			Second $\mathrm{n}\pi^*$		
E^a	E^d_{FC}	character	E^a	E^d_{FC}	character	E^a	E^d_{FC}	character
4.47	4.79	$\pi_H\pi^*_L$	4.69	5.36	$\mathrm{n}_N\pi^*_L$	4.66	5.20	$\pi_H\pi^*_L$
5.17	5.83	$\mathrm{n}_O\pi^*_L$	5.21	4.85	$\pi_H\pi^*_L$	4.81	5.91	$\mathrm{n}_O\pi^*_L$
5.44	5.35	$\mathrm{n}_N\pi^*_L$	6.16	5.86	$\pi_1\pi^*_L$	5.95	5.52	$\mathrm{n}_N\pi^*_L$
5.67	5.79	$\pi_1\pi^*_L$	6.15	5.86	$\mathrm{n}_O\pi^*_L$	6.20	5.81	$\pi_1\pi^*_L$
5.93	5.65	$\pi_H Ry_\sigma 1$	6.48	5.68	$\pi_1 Ry_\sigma 1$	6.09	5.94	$\mathrm{n}_O\pi^*_2$
6.18	6.05	$\mathrm{n}_O\pi^*_2$	6.68	6.77	$\mathrm{n}_N\pi^*_2$	6.51	6.10	$\pi_H Ry_\sigma 1$
6.34	6.08	$\pi_1 Ry_\sigma 1$	6.85	6.24	$\pi_1 Ry_\sigma 2$	6.88	6.53	$\pi_H Ry_\sigma 2$

Dark states in the FC point show mixed character. For this reason we parametrized new LVC Hamiltonians in the minima of some excited states, where they have a clear $\mathrm{n}_N\pi^*_L$ or $\mathrm{n}_O\pi^*_L$ character. The new parametrizations help us to have a clearer picture of the character of states populated during the dynamics. They have been performed with CAM-B3LYP in the minimum of $\pi_H\pi^*_L$ (here after labeled as LVC|Min-$\pi_H\pi^*_L$), of the first $n\pi^*$ state with $n_N\pi^*_L$ character (here after labeled as LVC|Min-$n_N\pi^*_L$) and of the second $n\pi^*$ state with $n_O\pi^*_L$ character (here after labeled as LVC|Min-$n_O\pi^*_L$). For better clarity therefore the LVC Hamiltonian at the FC point will be labeled as LVC|FC. The time evolution of population for all three cases show a sudden loss of population of the $\pi_H\pi^*_L$. This is explained by the coupling of the two bright states in the FC point where the initial wave packet is located.

Predictions of LVC|Min-$n_N\pi^*_L$ and LVC|Min-$\pi_H\pi^*_L$ Hamiltonians for an excitation to $\pi_H\pi^*_L$ are quite similar to those of LVC|FC. The only noteworthy difference

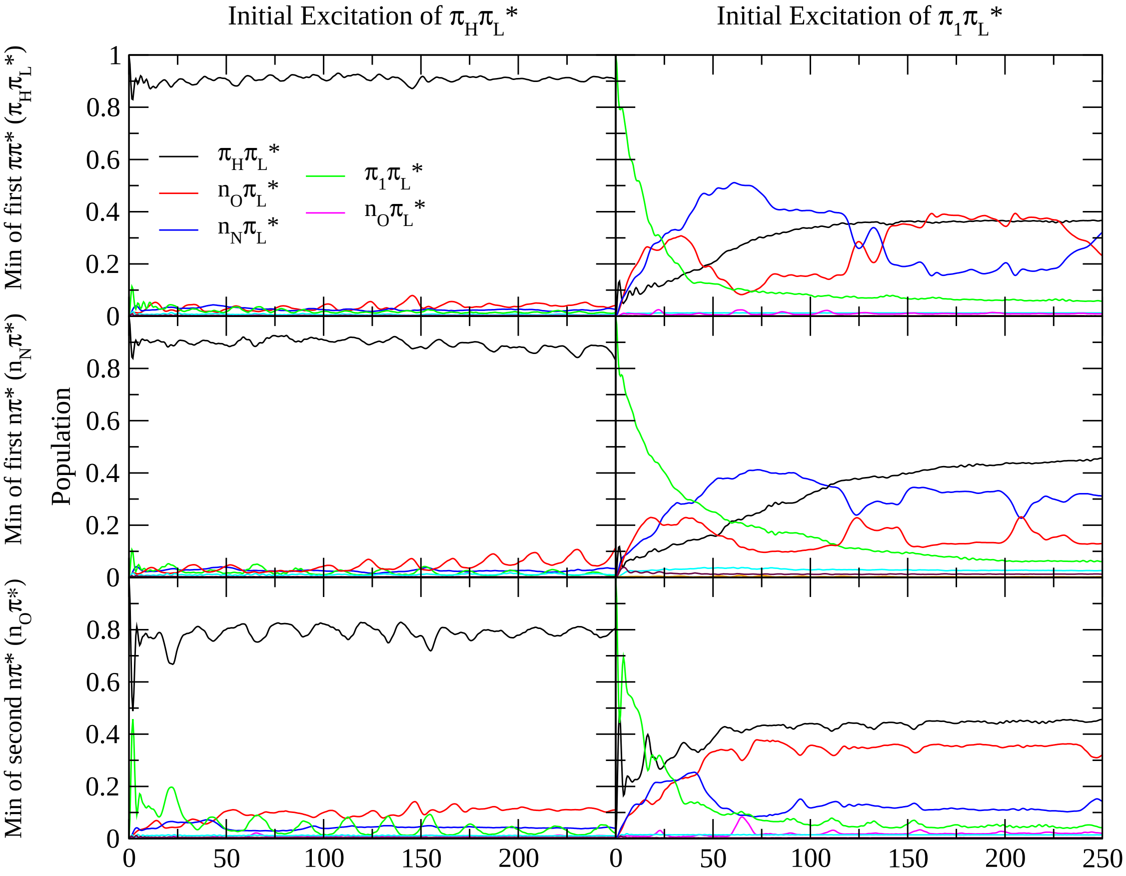

Figure S41: Nonadiabatic dynamics of electronic populations of 1,5diMe-Cyt in gas phase, as predicted by a LVC Hamiltonian parameterized with calculations at the $\pi_H\pi_L^*$ (top) $n_N\pi_L^*$ (middle) and $n_O\pi_L^*$ (bottom)C$_s$ minimum using CAM-B3LYP functional. Initial photoexcitation to $\pi_H\pi_L^*$ (left) or $\pi_1\pi_L^*$ (right).

is observed for the LVC|Min-$n_O\pi_L^*$. In fact, according to LVC|Min-$n_O\pi_L^*$, ~20% of the initial population flows to other states where the population of the $n_O\pi_L^*$ reaches ~10% of the total population which is 2 times larger than the population of $n_O\pi_L^*$ predicted by LVC|Min-$n_N\pi_L^*$ and LVC|Min-$\pi_H\pi_L^*$.

Considering an initial excitation to $\pi_1\pi_L^*$, the only noteworthy difference is that while for parameterizations at n$_N\pi^*$ and $\pi_H\pi_L^*$ minima (like for the one at the FC position) both n$_N\pi^*$ and n$_0\pi^*$ are remarkably populated and the wavepacket oscillates between them, it mainly localizes on the n$_0\pi^*$ state according to a LVC parameterized at the n$_O\pi^*$ minimum.

S3.5 Dynamics with a LVC model with quadratic correction of the PES of $\pi_H\pi_L^*$ state along the C=O stretching

Here we report the results of the quantum dynamical calculations with the "LVC-frequency-shift" Hamiltonians obtained by introducing a quadratic correction to the frequency of mode 42 on the $\pi_H\pi_L^*$ diabatic state according to what described in Section S2.3.2 of this ESI. Figure 42 compares the time-evolution of the electronic populations predicted with the original (solid lines) and modified (dashed lines) Hamiltonians at CAM-B3LYP (left panels) and PBE0 (right panels) level of theory, after an excitation to either $\pi_H\pi_L^*$ (top panels) or $\pi_1\pi_L^*$ (bottom panels). Changes are negligible for CAM-B3LYP and an excitation to $\pi_H\pi_L^*$, since the WP only moves on $\pi_H\pi_L^*$ and the displacement along the C=O stretching is limited. Differences for a dynamics initiated on $\pi_1\pi_L^*$ are moderate for CAM-B3LYP and mainly concern the populations of the two nπ^* states that cross at $\sim$ 150 fs. This is similar to what happens with a LVC parametrized at the $\pi_H\pi_L^*$ minimum (check Figure S41). Differences are instead remarkable with the PBE0 Hamiltonian. After an initial excitation to $\pi_H\pi_L^*$ the population transfer to the two nπ^* states is reduced, especially to the state n$_O\pi_L^*$−n$_N\pi_L^*$ more displaced along the C=O coordinate. This result can be explained noticing that, right after the photo-excitation, a significant population transfer to the n$_O\pi_L^*$−n$_N\pi_L^*$ takes place (similar for the original and modified LVC Hamiltonians). As a consequence, the WP starts moving along the coordinate connecting the GS and n$_O\pi_L^*$−n$_N\pi_L^*$ minima. Due to the quadratic correction, the $\pi_H\pi_L^*$ increases its stability (for large value of this coordinate) and therefore the population transfer is smaller. The same explanation holds for a dynamics initiated on $\pi_1\pi_L^*$, where after a similar initial increase of the $\mathrm{n}_O\pi_L^*-\mathrm{n}_N\pi_L^*$ population, the population of $\pi_H\pi_L^*$ becomes remarkably larger according to the LVC with the quadratic correction. Very interestingly, Figure S43 shows that thanks to the quadratic correction, the two lowest LVC adiabatic potentials at the average position of the WP are now very similar to the TD-DFT ones for the PBE0 parametrization, improving the agreement obtained with the original Hamiltonian (compare Figure S43 and Figure S24).

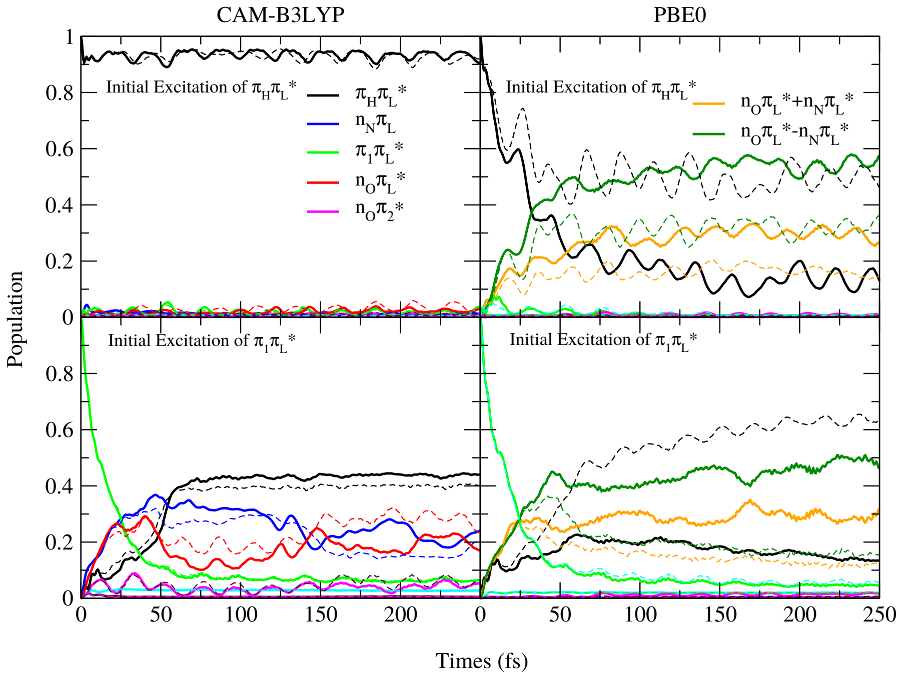

Figure 42: The time-evolution of the electronic populations reported in the main text for 1,5diMe-Cyt in gas-phase with a LVC parameterized in the FC position (solid lines) is compared with the results (dashed lines) when the frequency of mode 42 is decreased for CAM-B3LYP (left) and PBE0(right) calculations.

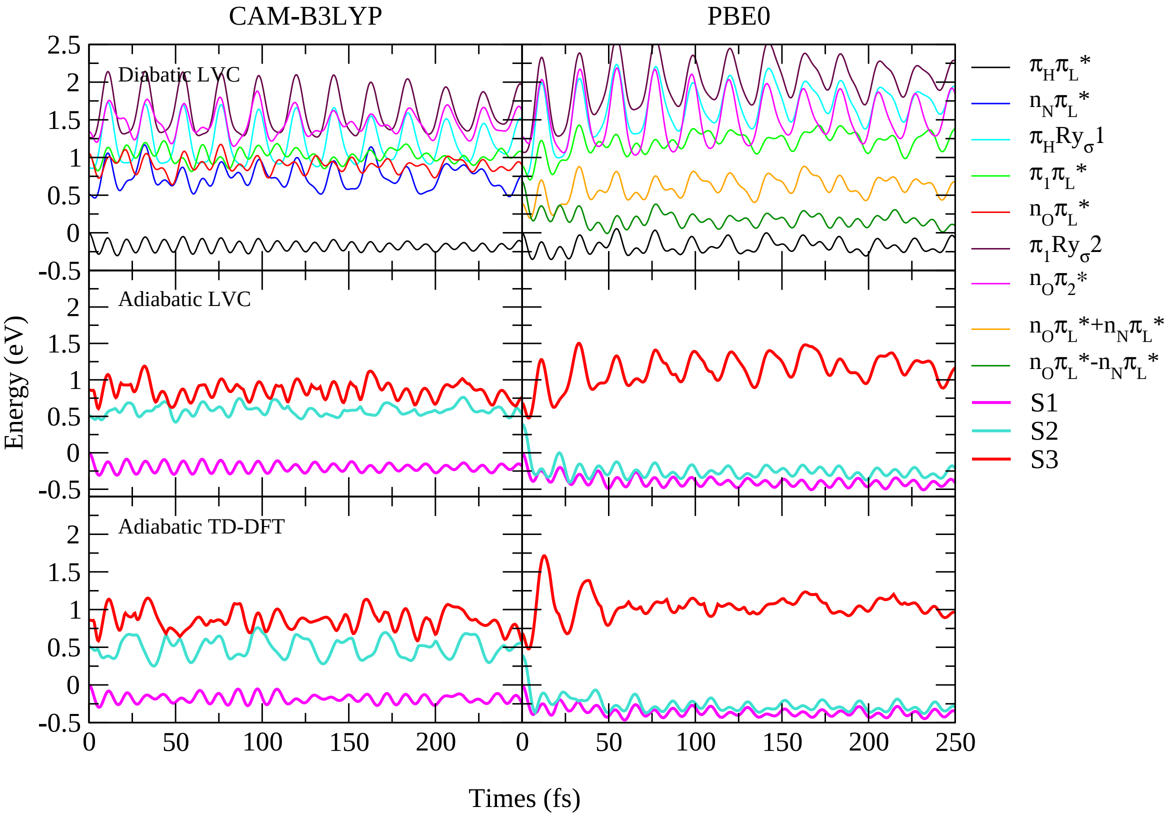

Figure S43: Diabatic (top) and adiabatic potential energies (middle, only for the three lowest states) in the average position of the wavepacket (C_s symmetry) obtained by LVC Hamiltonians parameterized with CAM-B3LYP (left) or PBE0 (right) calculations when the frequency of mode 42 is decreased. For comparison we also report (bottom) the three lowest adiabatic energies recomputed by TD-DFT at molecular structures corresponding to the average position of the wavepacket.

References

(1) Santoro, F. $\mathcal{FC}classes$, a Fortran 77 code, visit: www.pi.iccom.cnr.it/fcclasses, last consulted May 2018. 2008.